5-2012

Cellular Trafficking of Single and Multistage Vectors

Silvia Ferrati

Cellular Trafficking of Single and Multistage Vectors

by

Silvia Ferrati

M.S. Chemistry, M.S. Nanotechnology

_____

Supervisory Professor: Mauro Ferrari, Ph.D.

_____

Rita Serda, Ph.D.

_____

David Gorenstein, Ph.D.

_____

Craig Logdson, Ph.D.

_____

Andrew Bean, Ph.D.

APPROVED:

_____

Dean, The University of Texas
Graduate School of Biomedical Sciences at Houston

Cellular Trafficking of Single and Multistage Vectors

A

DISSERATION

Presented to the Faculty of
The University of Texas
Health Science Center at Houston
and
The University of Texas
M. D. Anderson Cancer Center
Graduate School of Biomedical Sciences
in Partial Fulfillment

of the Requirements

for the Degree of

DOCTOR OF PHILOSOPHY

by

Silvia Ferrati

M.S. Chemistry, M.S. Nanotechnology

May 2012

Dedication

This dissertation is dedicated to the memory of my grandpa who always supported me and encouraged me to persist in achieving my goals.

Acknowledgments

First of all I wish to thank my family in particular my mom, dad, brother, grandmother, uncle Stefano, aunt Daniela and cousin Viviana; all my achievements in my life are due to their support and love.

I am thankful to my advisors Dr. Ferrari and Dr. Serda for their help and guidance without which this work would have not been done. Their knowledge of the field, and their attitude and passion for their job motivated me to persist in my professional goals. I would also like to thank my graduate committee members Dr. Andrew Bean, Dr. Craig Logdson and Dr. David Gorenstein, for the time they dedicated to me and their useful critiques which helped me during these years.

I am also thankful to Dr. Xuewu Liu and Dr.Ciro Chiappini for porous silicon particles fabrication, Dr. Biana Godin for her contribution on the toxicity study, Aaron Mack for his technical assistance in particles modification and ICP measurements, Kenneth Dunner for his contribution with TEM microscopy, Dr. Jared Burcks for the help with live imaging experiments and Matt Landry for the help with figures and journal covers.

I would also like to thank the all nanomedicine especially John Martinez, Meenu Srinivasan, Jason Sakamoto, Brandon Brown, and Beth Hickman, for the joyful lab environment they offered me. I was able to grow as scientist through their support, guidance and technical assistance.

Alessandro Grattoni, Nicoletta Quattrocchi, Enrica de Rosa, Angela Hsiao and all my Italian colleagues, deserve a special thanks for being not only wonderful colleagues, but also dear friends.

Finally, I would like to thank Jeff Schmulen, for his continued support and love. He was always next to me in the good and bad moments helping me to be strong and determined.

This research was supported by the Department of Defense grants DODW81XWH-07-1-0596 and DODW81XWH-09-1-0212; NIH RC2GM092599 and pre-doctoral CPRIT Innovative Thinking Fellowship.

Abstract

Cellular Trafficking of Single and Multiple Vectors

Publication N° _____

Silvia Ferrati, Ph.D.

Supervisory Professor: Mauro Ferrari.Ph.D.

Nanomedicine is an innovative field of science which has recently generated many drug delivery platforms with exciting results. The great potential of these strategies rely on the unique characteristics of the devices at the nano-scale in terms of long time circulation in the blood stream, selective accumulation at the lesions sites, increased solubility in aqueous solutions, etc.

Herein we report on a new drug delivery system known as a multistage system which is comprised of non-spherical, mesoporous silicon particles loaded with second stage nanoparticles. The rationally designed particle shape, the possibility to modulate the surface properties and the degree of porosity allow these carriers to be optimized for vascular targeting and to overcome the numerous biological barriers found in drug delivery.

In this study we investigated the intra and inter cellular trafficking of the multistage system in endothelial cells bringing evidence of its bio-compatibility as well

as its ability to perform multiple intra and inter cellular tasks. Once internalized in cells, the multi-particle construct is able to dissociate, localizing in different subcellular compartments which can be targeted for exocytosis. In particular the second stage nanoparticles were found to be secreted in microvesicles which can act as mediators of transfer of particles across the endothelium and between different endothelial and cancer cells.

Table of Content

Table of Figures

Abbreviations

APTES-3-aminopropyl-triethoxysilane

BSA- bovine serum Albumin

DI- Distilled water

EC- electrochemical-etching

EPR - enhanced permeability and retention

FITC- fluorescein isothiocyanate

GFP-Green Fluorescent protein

HMVEC- human microvascular cells

HUVEC- human humbellical endothelial cells

i.v.- Intravenous injection

IPA- isopropyl alcohol

MRI - magnetic resonance imaging

MSD- mean square displacement

MSVs-Multistage vectors

MVB- multivesicular bodies

PBS- phosphate buffer solution

PEG- polyethylene glycol polymer

PEI-Polyethyleneimine

PLGA- poly(lactic-co-glycolic acid)

RES- reticulo-endothelial system

RGD- Arginine-Aspartic acid peptide

S1MPs- stage one micro-particles

S2NPs- stage two nano-particles

SEM-scanning electron microscopy

SIN- silicon nitride

SPIOs- Super-paramagnetic iron oxide nanoparticles

TAT- transcription activated proteins

TEM-transmission electron microscopy

VEGF- vascular Endothelial Growth factor

WGA- wheat germ agglutining

1 Background

1.1 Nanomedicine

When we talk about nanotechnology we refer to engineered particles or devices that have at least one dimension between 1 to 100 nanometers (nm), but in a broader classification we can extend the dimensions to 1000 nm [1]. The underlying rationale for this area of study is that at the nano-level particles or devices gain functional and chemical-physical properties that are not found in the equivalent bulk materials. Nanotechnology has wide applications ranging from biosensors, microchips, molecular switches, etc. The application of this new field of science to medicine for treatment, diagnosis and monitoring of disease has been recently referred by the National Institute of Health in the USA as 'nanomedicine'.

Since cancer is a leading cause of mortality all around the world, there is an acute interest in developing new nanosystems to help find a cure for this malignancy [2]. A vast area of research is dedicated to developing new nano-delivery systems for pre-approved drugs, especially chemotherapeutic agents [2a, 3]. Nanotechnology applied to medicine has strong potential in helping to achieve the goal of delivering drugs to the site of lesion, at the right time in a controlled fashion and at an effective therapeutic concentration [2c, 4]. Ideally, these systems will permit a more specific accumulation of the drug at the lesion, therefore increasing its efficacy and reducing side effects. In particular, nanoparticles attract large amount of interest given their characteristic size and the possibility to conjugate them with targeting ligands [5] (peptides, antibodies, aptamers etc.) which selectively recognize cancer cells or tumor microenvironment such

as vasculature [6] or stroma [7]. For instance folate, [8] peptides such as RGD [9] and antibodies like anti-HER have been employed to target nanoparticles to the tumor site.

Most of the current chemotherapeutic agents are small molecules with a broad pharmaco-kinetics which also causes them to interact with healthy tissues causing side effects such as alopecia, nausea and bone marrow damage. In addition, these drugs are easily excreted by the body and, therefore, high-concentration injections are required to assure the therapeutic efficacy dosage, further increasing the toxicity. Most chemotherapeutics are also hydrophobic molecules and are currently administered solubilized in solvents that are toxic, such as cremophor EL.

In conventional nano-micro drug carriers, the therapeutic agent is encapsulated or attached to particles which facilitates the solubility of the drug in aqueous solvents and protects the drugs from enzymatic degradation, improving its stability. Moreover, the encapsulation in particles combined with the targeting agents, facilitates cellular uptake enhancing drug accumulation at the target site.

Many types of nanoparticles for drug delivery, imaging and diagnostics have been developed in the past two decades, in particular, liposomes, polymeric nanoparticles, micelles, Qdots, dendrimers, gold, super-paramagnetic iron oxide, silica and silicon particles. Doxil and Abraxane are two well-known FDA-approved chemotherapeutic nano-formulations already available on the market. Doxil is the liposomal formulation of doxorubicin used for many types of cancers such as leukemia, breast, lung and ovarian [10]. Abraxane is instead a water soluble formulation of paclitaxel complexed with albumin nanoparticles which avoid the use of the toxic solvent Cremofor [11]. Nanomedicine has also improved the delivery of genes [12] and

siRNA [13] [14] offering an alternative to viral vectors. Nanoparticles conjugated to transcription activated proteins (TAT) are rapidly and efficiently delivered to the perinuclear localization in cells improving gene expression. In 2008 a phase I clinical trial was conducted to study intravenously injected polymeric targeted nanoparticles containing siRNA on patients affected by solid tumors[15]. The trials showed a significant down-regulation of the specific gene of interest. Inorganic nanopaticles such as Qdots [16] and superparamagnetic iron oxide [17] (SPIOs) have instead been extensively studied as imaging contrast agents. Qdots present several appealing characteristics for imaging such as the ability to tune their fluorescent emission, a broad absorption range, a high quantum yield and almost negligible photobleaching. On the downside their application *in vivo* is limited by their toxicity [16] which makes optimized coatings necessary. Super-paramagnetic iron oxide nanoparticles (SPIOs) on the contrary are made of biodegradable iron and their surface can be coated with various polymers that allow further conjugation of targeting molecules [18]. SPIOs are currently available in various sizes and are used as contrast agents for magnetic resonance imaging (MRI) [19].

1.2 Biological Barriers

Both drugs and particles have to bypass multiple biological barriers before reaching the target site [20]. Among these barriers there are: sequestration by the reticulo-endothelial system (RES), transport across vascular endothelium or gastrointestinal epithelium, diffusion in the stroma and crossing of cell and subcellular organelle membranes [21]. As a result, only a minimal percentage of the drug reaches the lesion site while the largest percentage accumulates in healthy organs, causing side effects.

These processes involve mass transport at multiple levels and in order to understand the mechanisms that govern transport across these biobarriers and develop more effective therapeutics it is necessary to bridge different scientific fields such as biology, chemistry, physics and mathematics. In this regard nanomedicine, which is per se a multi-disciplinary field, has brought an important contribution to the field of drug delivery, developing carriers that, given to their small dimensions and unique surface properties, have been able to reduce macrophage uptake and increase drug accumulation at the tumor site. However, a deeper understanding of the 'oncophysics' is necessary to develop more refined carriers and devices in order to successfully overcome these biological barriers and fight cancer.

1.2.1 Endothelial Barrier

In order to reach the tissue level the injected drug/carriers have to leave blood circulation and cross the endothelial barrier. The endothelial cells lining the blood vessels constitute a size-selective semipermeable barrier that tightly controls the diffusion of molecules from the blood to the interstitial space [22]. Two major mechanism of transport across the endothelial barrier have been identified: a paracellular pathway across the cell junctions and a trancellular pathway through the cells.

The junctions between endothelial cells are mostly constituted by (VE)-cadherin bound to catenins, an interaction that is crucial for the regulation of permeability [23]. The determination of molecules that can passively cross the blood vessel walls depends on the organ and type of endothelium. The brain, for instance, presents virtually no fenestrations while the remaining peripheral endothelium (capillaries) presents a cut off of 6nm which allow small molecules to pass through the junctions between cells [24].

Less continuous capillaries are also found in the kidney and liver with openings that can reach 40-50nm [25]. In the presence of inflammation or disease, like cancer [26], mediators such as VEGF disrupt intracellular-junction organization, causing larger fenestrations up to 2 μm, which make tumor blood vessels more permeable than regular organs. In addition, tumors present a defective lymphatic system which contributes to the enhanced permeability and retention (EPR) effect responsible for the increased accumulation of macromolecules and fluids in the tumor region [27]. Many drug delivery systems, such as liposomes, exploit this unique pathophysiology of the cancer vasculature to passively target particles of 100-150nm to the tumor site [27b, 28].

The transcellular pathway is mostly exploited by macromolecules larger than 3nm [25]. This mechanism, also known as receptor mediated transcytosis or carrier mediated transport, involves the interaction of the cargo with transporters or receptors expressed on the endothelium surface [22a]. Caveola, which is a membrane protein expressed in 70% of the capillaries, is the major vesicular transporter in endothelial cells. Caveola's interaction with the cargo activates a mechanism of endocytosis with membrane invagination of 50-100nm in size (caveolae) which pinch off creating vesicles that traffic across the endothelial barrier, transporting the cargo. The study of these types of interactions can provide ways to exploit these receptors and selectively transport carriers and drugs across the endothelium [29]. Thus a new generation of nanoparticles involves the functionalization of the carriers with moieties that improve these specific interactions which increase accumulation at the target site. A good example is Abraxane, in which the interaction of albumin with the gp60 endothelial cell membrane protein was exploited to facilitate the transport of the therapeutic agents to

the tumor site [11]. Along the same lines, recently cRGD conjugation on doxorubicin polymeric micelle has been shown to improve uptake by tumor endothelial cells overexpressing $\alpha_v\beta_3$ integrins [30].

1.2.2 Stromal Barrier

Once extravasated from the blood stream, the carriers encounter the stroma which constitutes an additional barrier to the penetration of the particles inside the tissue [31]. Multiple factors affect this transport-step, in particular the degree of vascularization of the organ, the extracellular matrix composition [32], the presence of inflammatory cells and the cell density [32-33]. All these factors affect the tortuosity of the path that the carriers have to perform to reach the target cells [31]. Moreover the stroma not only reduces the diffusion of the therapy in the tissue and therefore its efficacy, but because of the complex network of interactions between cancer cells and the tumor environment, promotes tumor growth providing a permissive environment in terms of nutrients, soluble factors, differentiation stimuli and fluid exchange.

The critical importance of these interactions was first proposed by Paget in 1889, when he suggested the 'soil and seed' theory [34]. He hypothesized that the tumor cells are like seeds that prefer to grow in hospitable soil. Now this idea is well recognized and evidence of the stroma's influence on angiogenesis, tumor growth, invasion and metastasis have been reported. Each tumor type presents, however, a characteristic stroma which can offer specific targets for therapies and potential markers for disease prognosis. For instance, a high level of tumor-associated macrophages has been correlated with poor prognosis for glioblastoma and breast cancers [35], or the extensive fibrosis in pancreatic cancer has been associated with the highly malignant

phenotype of the disease [36]. Anti-angiogenic therapies developed to block VEGF pathway [37], such as Avastin, fall into the category of therapies that target the tumor environment and have shown good results. Another example is anti-TGF agents that target pancreatic stroma in order to reduce the fibrosis and improve chemotherapy efficacy [38].

1.2.3 Cellular Barrier

Many drugs elicit their efficacy once internalized in cells, acting on specific intracellular organelles. Therefore, once the carriers reach the target cells, they will encounter the cellular membrane as the next barrier. There are several mechanisms by which a particle can be taken up by a cell, such as endocytosis, phagocytosis and clathrin – dependent or clathrin – independent endocytosis.

Different characteristics of the carriers such as size, charge, shape and material can dictate which pathway will be preferred and this will influence the final localization of the carrier inside the cell and its potential toxicity. Understanding how these factors influence the uptake and the intracellular trafficking of nanoparticles is helpful in order to rationally design carriers. Particles smaller than 500 nm can be internalized by cells through endocytosis [39]. The presence of specific ligands on the particles can further target them through this pathway triggering receptor mediated endocytosis. In both cases the cell membrane invaginates, creating vesicles (called cavaeolae) presenting a size up to 500nm, which will encapsulate the particle or macromolecule, transporting them inside the cell [40]. Particles bigger than 1μm are instead internalized by phagocytosis which requires the elongation of the cellular membrane (pseudopodia) in order to reach and engulf the particles [39]. Clathrin-mediated endocytosis also involves

the interaction of the cargo with specific membrane adapter proteins which trigger the invagination and formation of clathrin-positive vesicles which mediate the particle transport inside the cells [40]. For all the above pathways, once the vesicles are formed and internalized, they fuse with late endosomes and subsequently with lysosomes as part of their traffic toward perinuclear localization [41]. Clathrin-independent traffic instead avoids this fusion.

Not only the size, but also the particle geometry can influence the mechanism and rate of uptake. A systematic study conducted with macrophages correlated particles size and shape with three potential up-take outcomes: successful phagocitosis, attempted phagocytosis and unsuccessful phagocytosis [42]. The initiation of internalization was driven by Ω, defined as the angle between the particle and the cell membrane (correlated to the shape), but the completion of the process was shown to be regulated by the volume of the particle. Moreover, since phagocytosis requires a massive energy-consuming actin rearrangement with the formation of pseudopodia that surround the particle following its geometry, particles whose geometry requires less expansion of actin are more easily internalized. Mathematical models, integrating particle-physico-chemical characteristics with biological parameters such as vascular transport and margination have also been developed in order to predict the degree and rate of particle uptake [43]. Using these models, maps predicting the propensity of a given carrier to adhere and be internalized by cells were developed.

Targeting moieties based on receptors or antigens overexpressed on diseased cells or associated vasculature can also be used to direct the internalization through receptor-mediated endocytosis [9b, 39]. Among the several methods available to find

signature markers, there is the *in vivo* phage display[44], which has been used to identify various tumor endothelial cell markers such as $\alpha_v\beta3$ and $\alpha_v\beta5$ integrins, CRKL, GRP78, etc. Other targets such as the folate receptor [8], LHRH receptor [45] and PSMA [46] [47] are instead expressed on tumor cells. Liposomes conjugated to folic acid have been shown to be internalized by tumor cells faster through endocytosis compared to naked liposomes, proving increased up-take specificity. Many folate-based carriers have been recently developed and are currently undergoing testing in clinical trial. LHRH peptide has been instead used to target campothcin to ovarian, breast and prostate tumors [48]. Along the same line, a PSMA-targeting aptamer has been used to target PLGA-PEG nanoparticles- containing cis-platinum to prostate cancer cells [49].

1.3 Secretion of Nanoparticles

Even if nanoparticles have shown great promise as drug carriers there are still several fundamental problems that have to be understood and solved in order to refine their use. Intracellular trafficking of micro and nanoparticles has been extensively studied over the past decades. Particular interest has been spent in characterizing the endocytosis and intracellular localization of the particles, but less focus has been given towards investigating the long term retention of the particles in cells and their potential secretion into the surrounding area.

Nanoparticles commonly enter into cells through endocytosis or phagocytosis, resulting in their encapsulation in vesicles (early endosomes). These vesicles can then mature into late endosomes, also called multivesicular bodies, and subsequently fuse with either lysosomes or autophagosomes, in a complex pathway which creates various

types of intracellular vesicles: amphisomes, autolysosomes and lysosomes [50]. Hypothetically, at any point, the pathway vesicles can be recycled to the cellular membrane and released outside. Depending on the size and morphology, the secreted vesicles are classified as: exosomes [51], less than 100nm in size, released by a wide range of mammalian cells such as the cells of the immune system; microvesicles [52], 100nm-1μm, released by stimulated cells; and apoptotic bodies, larger than 1μm, released at the end of cellular apoptosis. A few studies have reported the exocytosis of nanoparticles such as PLGA[53] and iron oxide particles[54] and single walled nanotubes[55], opening a new, interesting field of research. The process is dynamic and it is hard to precisely quantify the rate of endocytosis and exocytosis at the same time. Through microscopy and single particle tracking Jin et al. has shown that the rate of exocytosis closely matches the rate of the internalization of particles[55]. In the context of endothelial cells, the exocytosis of PLGA particles in human vascular smooth muscle cells has been reported [53], showing that the process depends on the presence of serum in the medium. This suggests the involvement of opsonization in directing the internalized nanoparticles through the exocytic pathway. However, the mechanism by which these particles are released and the extent of this phenomenon across different cell lines is still not clear.

Gauze [54c] et al. have shown that iron oxide nanoparticles can be released in micro-biovesicles by macrophages, which are known to be able to shed their membrane in physiological and pathological conditions such as stress, apoptosis or upon activation, creating bio-vesicles which are released into the surrounding area. Similar evidence was found by Wilhelm et al. [56] which identified biovesicles containing SPIOs

released by eukaryotic cells. The nature of these nanoparticle-loaded vesicles, however, has not been investigated.

Many questions are therefore still unsolved and the impact of exocytosis and inter-cellular transfer of nanoparticles on their biodistribution, therapeutic efficacy and imaging characteristics.

1.4 The Multistage System

1.4.1 Strategy

Drug delivery carriers can be classified into 3 major classes: first generation carriers are naked particles, developed about a decade ago, that passively target tumor through EPR effect. Second generation particles added a level of complexity introducing surface decoration such as targeting moieties, environment-triggered activation, etc.; the third generation of carriers, instead, is composed of multiple nano-elements able to perform specific tasks in order to sequentially negotiate the biological barriers that they will encounter during their journey from the site of injection to the target lesion. Our multistage system (MSV) is an example of this class of carriers.

Our strategy is comprised of i.v. injectable stage 1 hemispherical nano-porous silicon micro particles (S1MPs) loaded with stage 2 nano-particles (S2NPs) [57]. S1MPs have been rationally designed through a mathematical model in order to optimize the three major processes that occur during the travel of the carrier in the blood stream: margination on blood vessels walls, adhesion on the endothelial cells and control of the internalization in cells [57-58]. Non spherical particles were shown to be the best candidates as carriers since they drift better toward the vessel walls increasing the

probability of interacting with it. The mathematical model was confirmed with *in vitro* experiments employing a parallel flow chamber and *in vivo* experiments in which particles presenting different shapes were injected into animals bearing breast cancer; these *in vivo* experiments showed hemispherical particles accumulated in the tumor in greater numbers [59].

Once docked to the vasculature of the lesion site, the S1MPs release their cargo which extravasates from the vasculature to reach the target. The schematic in Figure 1 summarizes the principle of our system. Porous silicon (pSi), was chosen as the material, since it is FDA approved and it is compatible with biological systems given the byproduct of its degradation is silic acid, a biologically harmless chemical. Moreover the size, shape and porosity of the material can be tightly controlled through semiconductor fabrication techniques therefore giving precise control over the final design [60]. In addition, the versatility of silicon chemistry allows the conjugation of the particles' surface with active targeting moieties, polymers such as poly(ethylene glycol) (PEG), etc. to increase circulation time and tumor accumulation [61].

The S2NPs loaded into the pores of the silicon carriers can be any type of nanoparticles from liposomes to micelle or polymeric particles which can also be loaded with therapeutic drugs, contrast agents or combinations of the two generating a vast selection of options. Metal nanoparticles such as SPIOs or gold can also be loaded and can function as contrast agents as well as thermo-ablation agents once the heat production is triggered by radio frequency or near infrared energy. This makes the system very versatile in terms of applications and possible payloads. Figure 2 recapitulates the possible types and combinations of S1MPs and S2NPs as well as

surface functionalizations and particle parameters to highlight this fundamental characteristic.

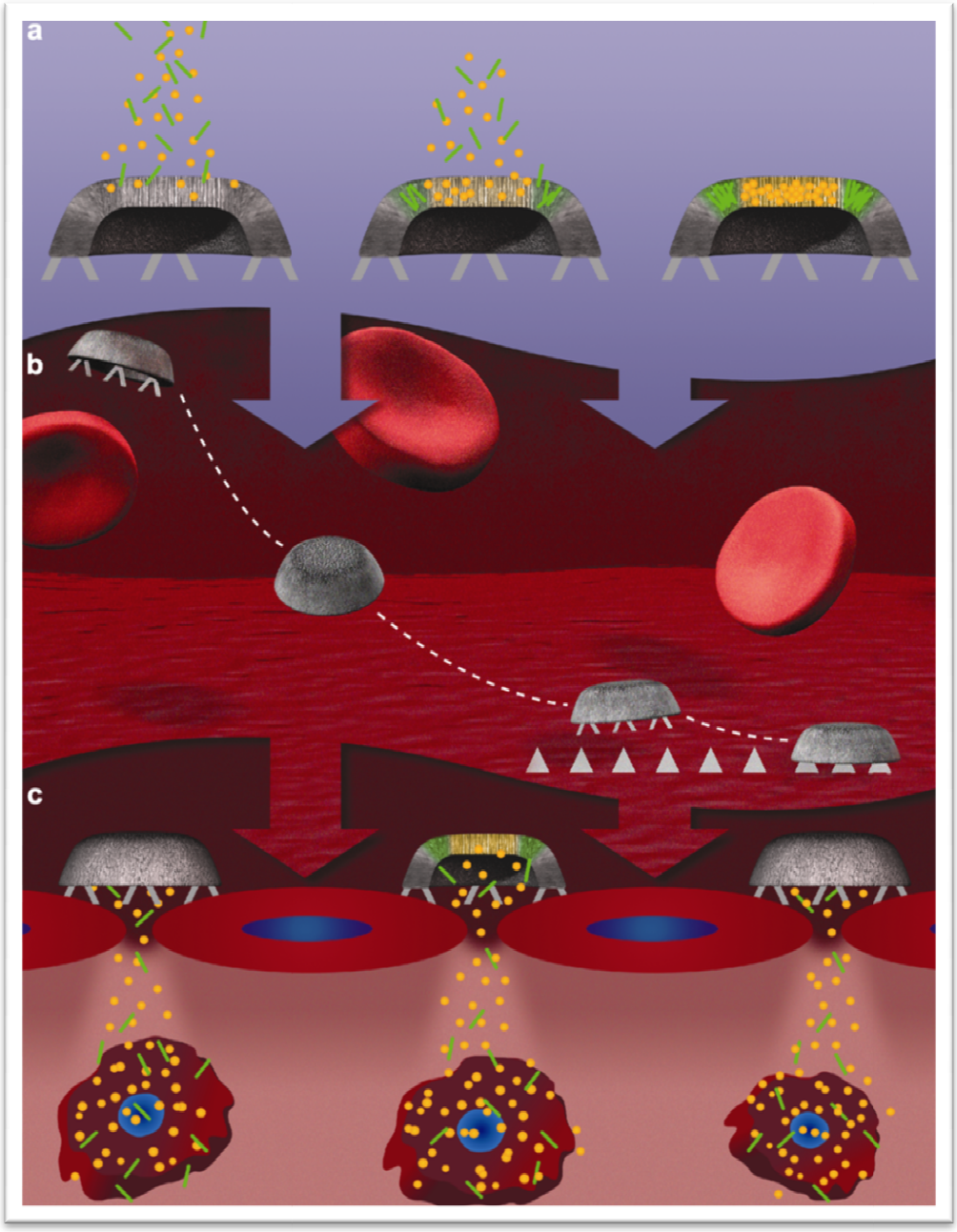

Figure 1 Schematic summarizing the principle of our multi-stage system. The S1MP porous silicon carriers are loaded with nanoparticles (S2NP) and then i.v. injected. After docking on the lesion vasculature the carriers release the S2NPs which cross the vasculature and reach the tumor cells *(Tasciotti et. al. Nature Nanotechnology, 2008, Courtesy of Nature Publishing Group).*

1.4.2 S1MP Fabrication

The fabrication of the S1MPs is comprised of a combination of photolithographic, reactive ion-etch, electro-chemical etch and particle release steps on heavily doped 100 mm silicon wafers (p++, (100), <0.005 Ωcm). The 3.2 μm hemispherical particles are made by first depositing a sacrificial layer of silicon-rich silicon nitride on the wafer. This is followed by a photolithography process using AZ5209 photoresist to imprint a pattern of 2 μm diameter circles using a chrome-plated mask. Then a series of reactive ion etches are applied to remove parts of the sacrificial silicon-nitride layer, exposing the surface of the wafer with 2μm holes. The photolithographic resist is then removed using a 'pirahna' solution after which the wafer undergoes an electro-chemical etch (EC-etch) to create the porous layers of the particles. The pore size, degree of porosity and thickness of the particles can be tuned during the EC-etch step by varying the electric current, chemical-solution concentrations and etching time. Based on the knowledge in fabrication protocols developed in our laboratories, and by modifying various parts of the standard process, we can produce particles with dimension ranging from 500 nm to 3.2 μm, with pores from 5 to 80+ nm, in both hemipherical and discoidal shapes. The high degree of porosity allows the loading of a large amount of S2NPs and, at the same time, control of their release profile based on particle degradation.

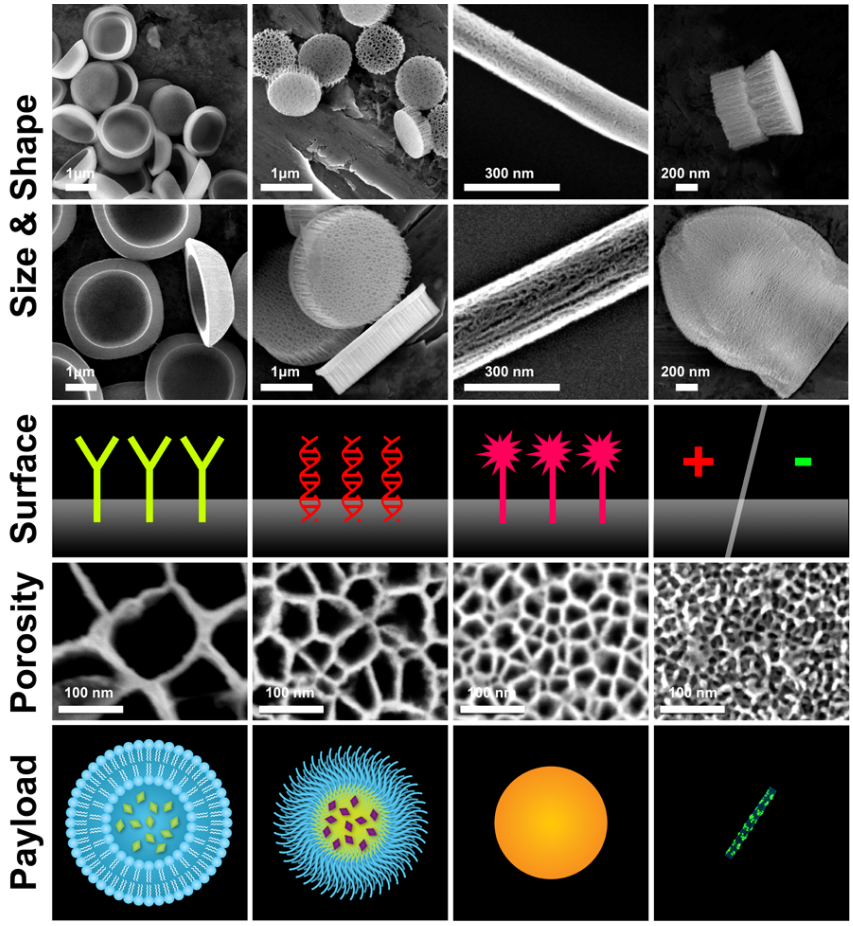

Figure 2 Versatility of our MSV in terms of size, shape, degree of porosity, surface properties (negatively and positively charge groups, PEG or other polymers, functionalization with antibodies, peptides, aptamers and fluorescent probes) and possible payloads (liposomes, micelles, inorganic/metallic nanoparticles, carbon nanotubes) *(Biana et al. Accounts of chemical research, 2011, Courtesy of ACS Publication).*

2 Methods

2.1 Cell Culture

Human microvascular endothelial cells (HMVECs) were received as a gift from Dr. Rong Shao (University of Massachusetts) and grown in EBM® medium, (CC-4133®, Lonza, Walkersville) while Human Umbilical Vein Endothelial Cells (HUVECS), bought from Lonza, Walkersville, Inc, were cultured in EBM®-2 medium (CC-3124® , Lonza, Walkersville).

Both cell lines were grown in monolayers 80% confluent in at 37C in 5% CO_2. Cells detachment was performed with 0.25% mg/ml trypsin solution (Clonetics).

2.2 Porous Silicon Particles and Surface Functionalization

Hemispherical silicon microparticles were manufactured by our group at the Microelectronics Research Center at University of Texas at Austin using lithographic techniques. Particles were produced in two sizes: 1.6±0.2 and 3.2±0.2 μm; with pores size ranging of 26±0.2 μm, for hemispherical one, and 53±0.2 μm for discoidal one.

Particles were heated at 110ºC in piranha solution (1 volume H_2O_2 and 2 volumes of H_2SO_4) for 2 hours to oxidize their surface and create a negative surface charge. Washing steps with deionized (DI) water were used at the end of the oxidation process before re-suspending the particles in isopropyl alcohol (IPA), where they are usually stored till their use. 3-aminopropyl-triethoxysilane (APTES) was employed to create a positive coating on the particles. The conjugation was conducted suspending the particles in a solution of 0.5% (v/v) APTES in IPA for 2 hours at room temperature. Both modifications were evaluated checking the particles surface charge by zeta potential. In order to functionalize the particles with poly(ethylene glycol) (PEG), APTES-modified particles were incubated for 1.5 hours with 10nM PEG-5000 (Laysan

Bio Inc.) in acetonitrile and subsequently washed with DI water to remove the un-conjugated PEG.

2.3 Scanning Electron Microscopy

$4x10^4$ cells were seeded on silicon chip supports (Ted Pella, inc, Redding, CA) in a 24 well plate. Upon confluence, cell were incubated for 15 min with 1.6 or 3.2 μm oxidized particles (ratio 10:1 particles per cell) at 37 ºC in serum-free medium. Cells were then washed with PBS, fixed with 2.5% glutardehyde (Sigma-Aldrich, Saint Louis, MO) and washed again in PBS. Samples were then dehydrated incubating in progressively more concentrated solutions of ethanol (30%, 50%, 70%, 90%, 95% and 100%) for 10 minutes each. As last step, cells were incubated 10 minutes with a solution of 50% (v/v) ethanol-hexamethyldisilazane (Sigma, Saint Luis, MO) followed by 5 minutes in 100% hexamethyldisilazane. Samples were dried overnight in a dessicator. Silicon chips were mounted on SEM stubs (Ted Pella, Inc. Redding, CA) with the help of conductive adhesive tape (12mm OD Pelco, Ted Pella, Inc. Redding, CA), sputtered with a 10 nm film of gold by means of a Plasma Science CrC-150 Sputtering system (Torr International, Inc.) and then they were imaged with a FEI Quanta 400 FEG-SEM (high vacuum conditions, 20kV, spot size 5).

2.4 Transmission Electron Microscopy

HMVECs were grown at a concentration of $1x10^6$ cells/well in a 6 well plate and then incubated 6 hours at 37 ºC with 1.6 and 3.2 μm hemispherical particles, either oxidized or APTES modified. After the samples were washed with PBS, the fixation step was performed with a solution of 2% paraphormaldehyde (Electron Microscopy Science, Hatfield, PA) and 3% glutaraldehyde (Electron Microscopy Science, Hatfield, PA) in

0.001 M phosphate buffer saline (PBS), pH7.4. Samples were then washed, treated with 0.1% Millipore-filtered cacodylate buffered tannic acid and then stained with 1% buffered osmium tetroxide for 30 min followed by 1% millipore-filtered uranyl acetate. The samples were subsequently dehydrated in progressively more concentrated solutions of ethanol (30%, 50%, 70%, 90%, 95% and 100%) and then infiltrated with Epon resin. The resin-embedded samples were let polymerized in an oven at 60 ºC for 2 days. A Leica Ultracut microtome (Leica, Deerfield, IL) was employed to obtain Ultrathin sections of the samples which were then stained with uranyl acetate and lead citrate in a Leica EM Stainer. Images were acquired with a JEM 1010 transmission electron microscope (JEOL, USA, Inc., Peabody, MA) with a voltage of 80 kV.

The same procedure was used to investigate the trafficking of the MSV and SPIOs in endothelial cells. For the first experiment, HMVECs were grown in a 6-wells plate till 80% confluence, were then incubated with the assembled MSV system for 24 hours (5:1 particles/cell) and then processed for TEM. For the second experiment, HMVECs were plated at a concentration of $1x10^6$ cells/well in a 6 well plate and then incubated 6 hours with PEI-SPIOs (7μg/ml). Cells were subsequently fixed and processed for TEM imaging. The same protocol was also carried out with HMVECs, 4T1 and MCF7 cells, after incubation overnight with microvesicles concentrated from the HMVEC's supernatants well as with the concentrated microvesicles pellet.

2.5 Confocal Microscopy

HUVECs were let adhere overnight on 1.5 mm glass coverslips and then they were treated with 3.2 μm silicon particles (5:1 particles to cell ratio) for 2 hours at 37 ºC. After being washed with PBS, cells were fixed with 4% paraphormaldehyde,

permeabilized with a solution of 0.1% Triton X-100 and blocked with a solution of 1% Bovine Serum Albumin (BSA) in PBS. Cells were then stained with 200 nM Alexa Fluor 555-Phalloidin (Invitrogen, Carlsbad, CA). Coverslips were then mounted on a confocal glass slide using Vectashield mounting media (Vector Laboratories, Burlingame, CA). Images were acquired with a Leica DM6000 confocal microscope with a 63x oil objective. Particles were visualized using auto-fluorescence exciting with a 633 laser.

In order to characterize the mechanism exploited by our particles to traffic inside cells, HMVECs were grown till 80% confluence on 1.5 mm glass cover slips and then they were incubated with 3.2 μm silicon particles for 5 hours. The behavior of cell in regular medium was compared to cells grown in medium containing 150 nM nocosazole (Sigma, St. Luis, MO). Cells were processed for confocal following the standard procedure of fixation, permeabilization and blocking as previously reported. FITC-labeled anti-α-Tubulin monoclonal antibody (Abcam) at 1:200 dilutions was employed to stain the cell microtubules. Nuclei were stained with DRAQ5 (Biostatus Ltd) at 1:1000 dilution. Coverslips were then as usual mounted on a confocal glass slide using Prolong Gold as mounting media (Vector Laboratories, Burlingame, CA). Images were acquired with a Leica DM6000 confocal microscope with a 63x oil objective. Particles were visualized using bright field.

To confirm the particles co-localization with phagolysosomes we transfected a GFP-NPC1 construct (kind gift of Dr. J. Suh at Rice University) into cells with the help of an Amaxa Electroporator. $1x10^{6}$ cells were trypinized, resuspended in 100 μl of Amaxa HUVECs nucleofactor solution (Lonza, Walkersville, MD), combined with 5 μg of

DNA and transfected with the appropriate electroporator programmed ramp. Cells were then diluted in medium and immediately plated on a glass bottom dish. Upon reached confluency, cells were incubated for 2 hours with 3 different variation of paricles: 3.2 μm 594-dylight (Pierce)-conjugated particles 3.2 μm and 1.6 μm APTES-modified particles, then washed with PBS , fixed and imaged with an 1x81 Olimpus Microscope equipped with a 40x objective.

In order to investigate SPIOs trafficking in endothelial cells, $5x10^4$ HMVECs were plated on an 8 well glass bottom confocal chamber slide (BD Falcon) and left to adhere overnight. After cell membrane staining for 10 minutes at 37C with 594 wheat germ agglutining (WGA) (Invitrogen), cells were incubated with 488-dylight (Pierce) conjugated PEI-SPIOs (5μg/ml final concentration) overnight. The samples were then fixed with a 4% paraphormaldehyde solution, mounted with prolong gold mounting medium on confocal slides and imaged with a A1 Nikon confocal microscope.

For the staining of concentrated microvesicles, the pellet was instead fixed with 4% paraphormaldehyde solution, washed once with a solution of 0.1% BSA in PBS and then stained with Alexa Fluor 488-Lamp1 antibody, 1:50 dilution, (Santa Cruz Biotchnology) for 1 hour at room temperature. The pellet was then washed with PBS and incubated overnight with 4T1 breast cancer cells, previously seeded in glass bottom confocal chambers. 4T1 were then fixed with 4% paraphormaldehyde, mounted with prolong gold and imaged with a confocal Nikon microscope. Reflectance was used to visualize the iron oxide nanoparticles contained in the FITC-labelled vesicles.

2.6 Live Microscopy

For the live cell imaging, HMVECs ($25x10^3$ per well) were grown on a 24 well-glass bottom dish (Mat Tek corporation, Ashland MA). 3.2 μm or 1.6 μm APTES-modified particles as well as 3 variations of spherical silica beads (1, 2.5 and 3 μm) were added to the cells. The samples were visualized with a 1X81 Olimpus Micriscope equipped with a humidified 37 ºC incubator with 5% CO_2 , images of 5 focal planes were taken with a 20X at 5 minutes intervals for 19 hours. The more rapresentative shots are reported as still images, while the the remaning pictures were projected and compiled into movies.

Particles tracking was permormed using Slide Book software, analyzing the x and y coordinates of the particles over time. The mean square displacements (MSD) were calculated with the following equation:

$$\langle \Delta r^2(\tau) \rangle = \langle [x(t+\tau) - x(t)]^2 + [y(t+\tau) - y(t)]^2 \rangle$$

From which, through fittings, it was possible to calculate the rate of intracellular trafficking. Calculations and fitting were performed with Excel.

2.7 Fluorescence Microscopy

For the quantitative analysis of the mitotic trafficking of microparticles, HMVECs were grown in a petri dish and subsequently incubated with 488-dylight (Pierce)-conjugated 3.2 μm particles (10:1 particles/cell) overnight to ensure internalization. The population of cells presenting the highest fluorescence and therefore the higher number of particles/cell was selected with a Becton Dickinson FACS Diva Flow Cytometer and Cell Sorter (BD Bioscience, San Jose, CA). The sorted cells were then plated in glass bottom dish at 5 different concentrations, starting from 25000 cells and diluting 1:2 till 800 cells per well. Every 24 hour for 6 days, bright field and fluorescent images of the

cells were acquired with a fluorescent microscope (Nikon TS 200) with a 20x objective. The number of particles per cell was manually determined from the images.

2.8 Flow Cytometry

1.6 μm APTES-modified particles were conjugated to a pH sensitive dye (pH Rhodo-NHS Ester, Invitrogen, Carlsbad, CA), which becomes fluorescent in acidic pH. The conjugation between the carboxyl group of the dye and the amino group of the APTES-particles was conducted in DMSO directly adding the dye solution to the particles incubating for 2 hours at room temperature. Particles were then washed twice with DMSO and twice with IPA to remove the un-bounded dye. Cells, plated on a 6 well plate, were starved in serum-free medium for 40 minutes before adding the pH-Rhodo-particles at a 10:1 particles/ cells ratio. Plates were centrifuged at 1500 rpm to let the particles settle down before incubation at 37 ºC for different amounts of time. Cells were then trypsinized, fixed and analyzed with a Becton Dickinson FACS caliber and Cell Quest software.

2.9 Enzyme-linked immunosorbent assay (Elisa)

HUVECs, seeded at 50000 cell/well in 24-well plate, were incubated with either 3.2 μm APTES-modified particles or PEG-500 (5:1 particle/cell). 20 μg/mL zymosan was used as positive control for cytokines up-regulation. 100 μl of the cell medium was collected at different time points (1, 4, 24 hours) and stored at -80 ºC till analysis. The removed medium was each time replaced with fresh medium. Interleukin-6 (IL-6) and interleukin-8 (IL-8) were measured in the medium using the Human IL-6 and IL-8 ELISA Kits (Cell Science) following the manufacture protocol.

2.10 Tube Assay

HMVECs were pre-labeled by incubating them for 15 minutes at 37º C with orange cell tracker (Invitrogen, Carlsbad, CA). 4 x 10^4 labeled HMVECs were then seeded on 80 µl of matrigel (Geltrex, Gibco, Grand Island, NY) in a glass bottom confocal chamber slide (BD Falcon, San Jose, CA) in the presence or absence of 488-Alexa Fluor (Pierce-labeled 3.2 µm S1MPs and let adhere overnight. The slides were then imaged with a A1 Nikon confocal microscope equipped with a 20x objective.

2.11 Zeta Potential and Fourier Transform Infrared Spectroscopy (FTIR)

The surface charges of 15 nm amino-polyethylene glycol (PEG) polymer coated SPIOs nanoparticles (NH2-PEG SPIOs) (Ocean nanotech, Springdale, Arkansas) and oxidized silicon particles were tested with a Zeta Potential Analyzer (Zeta PALS). Three measurements were taken in both PBS (pH7) and borate buffer (pH5) and the final value reported was the average.

The qualitative analysis of the NH2-PEG SPIOs surface coating was performed with FTIR and compared to carboxylated SPIOs. Dried samples were applied directly to the on the diamond surface of a SMART ATR attachment on a Nicolet 6600 FTIR spectro-photometer. Data were collected with a resolution of 4cm^{-1} and as an average of 16 readings. The peaks analysis was performed with Omnic Peak Identification software.

2.12 Porous Silicon Particles Loading

In order to assemble the multistage system, 1x10 ^{7} 3.2 µm S1MPs were dried from IPA overnight and then incubated with 100 µg of 15nm SPIOs in borate buffer (stock solution 1mg/ml) for 30 min at room temperature. Samples were then washed twice with DI water to remove the un-loaded SPIOs. Porous silicon particles were recollected each time by centrifugation at 2000 rpm (Beckman Coulter Allegra X-22 Centrifuge

equipped with a 296/06 rotor). To evaluate the loading efficiency, we measured the content of iron in the washing solutions as well as silicon carriers pellet by means of inductively coupled plasma optical emission spectroscopy (ICP-OES) with a Varian Vista AX (power set at 1kW, plasma flow set at 15L/min, auxiliary flow of 1.5L/min and a nebulizer flow of 0.75L/min, 5 replicates).

2.13 Inductively Coupled Plasma Optical Emission Spectroscopy

In order to quantify the concentration of iron in the supernatant over time, HMVECs were seeded in a 6-wells plate, once reached 80% confluence, they were incubated with $3x10^6$ loaded MSVs per well. Free SPIOs (5μg) were used as comparison. After 12 hours cells were washed to remove particles not yet up taken and fresh medium was added to obtain the actual initial iron concentration. The amount of iron present in the medium at this time point was subtracted by the initial amount of iron added. Conditional medium was then collected over time at 1, 3, 5 and 7 days. Cells were split after 3 days and the media from the two wells were summed at the end before analyzing iron content. Collected samples were concentrated by centrifugation at 4200 rpm for 30 minutes and the pellets were then dissolved incubating with 10μl of 10-12 M hydrochloric acid, for 2 hours at 60 ºC shacking at 1300rpm. The samples were then brought to the same volumes (5ml) with spectrosol solution (CFA-C, Spectrosol Inc.) at pH8.5. Iron standards were prepared at concentrations of 10, 25, 50, 100, 250 and 1000 mg/L. Spectrosol solution was used as blank while a solution of iron at 125mg/L was used as the quality control standard.

50μl of an yttrium solution (stock solution 100mg/ml) were added to each samples and standard as internal reference. Iron content was quantified with a Varian Vista AX ICP-

OES (power set at 1kW, plasma flow set at 15L/min, auxiliary flow of 1.5L/min and a nebulizer flow of 0.75L/min, 5 replicates).

2.14 MTT Cell Proliferation Assay

HMVECs were seeded into 96-well plates (5000cell/well in 200 µl medium) and left to adhere overnight. Cells were then incubated with 15nm Polyetilenamine (PEI)-coated SPIOs (Ocean Nanotech) at a concentration of 2µg/ml for 24 hours. The medium was then replaced with fresh medium and cell proliferation was checked at 24, 48,36 and 72 hours adding 200ul/well solution of 3-(4,5-dimethylthiazol-2-yl)-2,5-diphenyltetrazolium bromide (MTT reagent, Sigma) at 0.5mg/ml. Cells were incubated with MTT reagent for 2 hours and then the solution was replaced with 200 µl dimethyl sulfoxide (DMSO). After 15 minutes incubation at room temperature absorbance was measured at 570nm with a Synergy H4 plate reader (BioTek).

2.15 Concentration and Magnetic Purification of Biovesicles

HMVECs cells were cultured in a T150 flask and once reached 80% confluence they were incubated with 2µg/ml PEI-SPIOs for 12 hours. The medium was then replaced with fresh medium to remove non uptaken particles. Conditional medium from the cells was then collected at day 3 and concentrated by centrifugation (21000xg 5 minutes). The brown pellet obtained was then re-suspended in PBS and further purified with magnetic separation overnight employing a magnet cuvette holder (Ocean Nanotech). The separated pellet, containing the SPIOs, was then processed for further experimenting as follow.

3 Results and Discussion

3.1 Intracellular Traffic of Porous Silicon Micron-Particles

3.1.1 S1MPs Uptake by Endothelial Cells and Micro-Tubules Mediated Transport

Like many particles carrying systems, our multistage system is i.v. injectable and therefore it will have to interact with endothelial cells, in order to reach the lesion site. Moreover, since the vasculature of many lesions, among which cancer, presents unique characteristics in terms of structure [27b] and markers [62], endothelial cells are often the primary target for the drug delivery systems [6, 63]. Therefore the study of the interaction of our system with endothelial cells is of fundamental interest to understand the mechanism of uptake and release of particles in cells as well as their biocompatibility.

We employed microscopy techniques and *in vitro* assays in order to characterize the mechanism of uptake, intracellular localization of the carriers and impact of particles presence on cellular morphology, viability and cell cycle. As a model for this study we choose two endothelial cell lines: human microvascular cells (HMVEC) and human umbilical endothelial cells (HUVEC). Size, shape and surface properties of the particles can influence their interaction cells and therefore the impact of these parameters on the mechanism of particle uptake was of particular interest for us. Endothelial cells acted as non-professional macrophages internalizing S1MP particles through a combination of phagocytosis and macro-pinocytosi. Both mechanisms relied on an extensive actin rearrangement that led to an actin cup formation which surrounded and engulfed the particles. The early steps in the internalization of particles

were documented in a previous work with scanning electron microscopy (SEM) micrographs[64]. The process looks similar for both 1.6 or 3.2 μm SIMPSs with cellular pseudopodia elongating and reaching the particles within 15 minutes incubation with HUVECs at 37ºC. The subcellular localization of S1MPs was investigated by transmission electron microscopy (TEM) and confocal microscopy. 1.6 and 3.2 μm silicon particles, positively and negatively charged, were employed for this experiment. The surface modification of the particles was achieved by oxidation with piranha solution and 3-amino-propyltriethoxysilane (APTES) conjugation, respectively. HMVEC cells were incubated with particles for 6 hours and then fixed and prepared for TEM. The micrographs show the internalized particles localized in vesicles (phagosomes). The magnifications in Figure 3 clearly show the tight membrane surrounding the particles, for both particles sizes (Same result were obtained for oxidized particles, data not reported). Confocal images of HUVECs incubated for 60 minutes with oxidized S1MPs and subsequently stained for actin were also acquired.

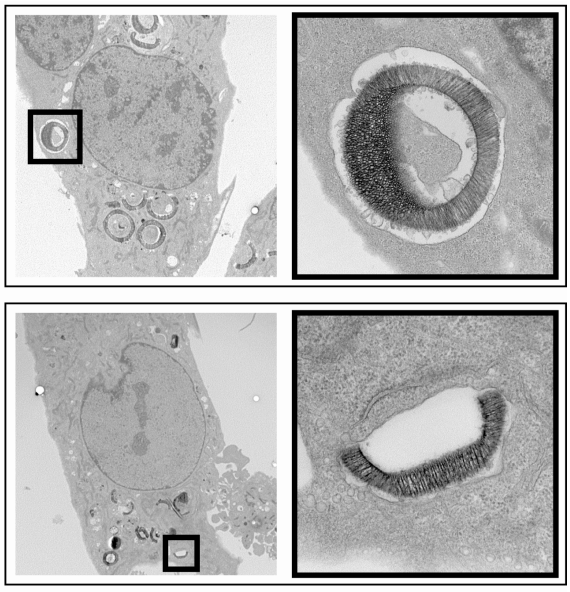

Figure 3 TEM micrographs of APTES modified particles incubated with HMVECs for 6 hours. In the top two images the particles are 3.2 μm in size while in the bottom two they are 1.6 μm in size. *(Ferrati et al.' Intracellular trafficking of silicon particles and logic-embedded vectors' Nanoscale 2010, Courtesy of RSCPublishing).*

Subcellular details, such as organelles and nuclei, displayed in TEM images appeared healthy. In addition the surface charge and size did not seem to influence the compatibility of the particles to be internalized by endothelial cells or the characteristics of the vesicular compartments that housed them.

Once formed inside the cell, the phagosomes fused with endosomes and later on with lysosomes in a process of maturation that requires the transient association of several different proteins on the vesicles membrane. EEA1 and Rab5 proteins play a role in the early stage of maturation while Lamp1 and NPC1 are recruited in the later stages. These motor proteins are necessary to traffic the phagosomes into the cells, docking them on the microtubules. This mechanism promotes a centripetal movement of the vesicles which brings them into the perinuclear area. In order to understand if our particles were moving inside the cells, exploiting the same trafficking mechanism, we incubated 3.2 μm S1MP particles with HMVECs cells for 6 hours in the presence or absence of 150 nM Nocodazole, which disrupts microtubules, thus inhibiting this specific trafficking mechanism. Cell nuclei were stained with DRAQ5 and the microtubules were stained with a FITC-labeled α-tubulin antibody. To evaluate the particles distribution in the cells with respect to the nuclei, cells were divided into quadrants presenting defined distances from the nuclei and the number of particles per quadrants was evaluated (Figure 4). The nocodazole-mediated disruption of microtubules reduced particles ability to accumulate in the perinuclear area by 80%. This provided insight into the intracellular mechanism of transport of the particles which resulted microtubules mediated and not randomly diffusive.

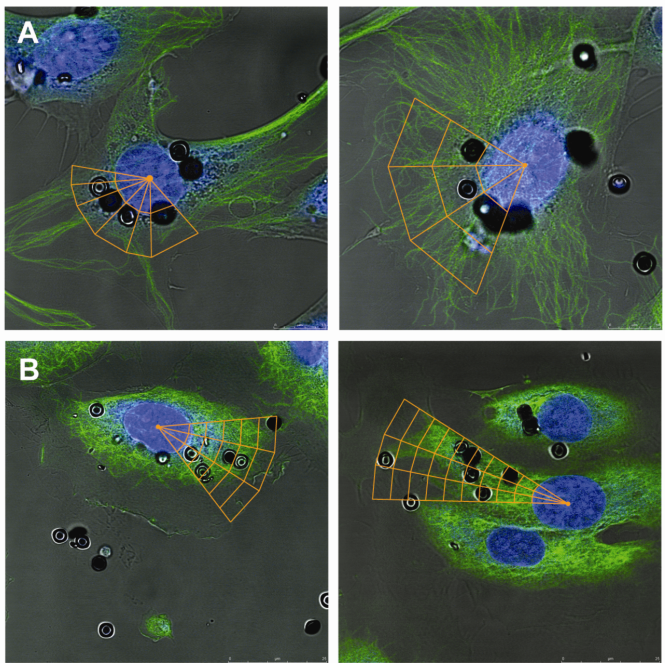

Figure 4 Confocal images of particles internalized with regular HMVECs (top figure) or nocodazole-treated HMVECs (bottom row). Cells were stained with a FITC-α-Tubulin antibody for microtubules and DRAQ5 for nuclei *(Ferrati et al. 'Intracellular trafficking of silicon particles and logic-embedded vectors' Nanoscale 2010, Courtesy of RSCPublishing).*

3.1.2 Maturation of Phagosomes Bearing S1MPs

A well-known property of mature phagosomes is their acidity. The pH of the vesicles slowly decreases from 7 to 5 as phagosomes fuse with late endosomes and lysosomes. To evaluate the integrity of the pathway and the long term fate of the internalized particles we conjugate a pH sensitive dye (pH Rodo, Invitrogen) on the surface of 3.2 μm silicon particles, which emits fluorescent light in acidic environments. We then tested the pH-Rhodo particles measuring the increase in fluorescence of the particles in solution presenting different pH levels. This confirmed an increase in fluorescence, from 2.2 to 27, passing from pH 7 to pH 4. We then tested these particles in HMVECs performing a time-course incubation experiment evaluating cell

fluorescence a different time points. This showed an increase in the mean fluorescent intensity of cells over time from an average of 5 at time zero, when the particles are still on the cell surface, up to an average of 19 after 16 hours of incubation (Figure 5 A). We observed a slightly decrease in intensity at 24 hours which may occur because of particles degradation or cleavage of the dye from their surface.

Overall this data indicates that the vesicle traffic machinery is not negatively affected by our particles and phagosomes containing S1MP are still able to mature and accumulate in the perinuclear region moving along the microtubules. To confirm particle co-localization with phagolysosomes we trasnfected HMVECs with a construct presenting GFP fused with Nieman Pick C1 (NPC1) in order to specifically label the lysosomes. Next we incubated the trasfected cells with Dylight 594-labelled 3.2 μm particles and imaged with confocal microscopy. Figure 5B shows the acquired images in separate and combined channels to highlight the GFP-NPC1 expression (the green ring) in the membrane surrounding the internalized particles, which suggests the localization of particles in lysosomes. Since the presence of the fluorophore on the particles could theoretically influence the intrinsic traffic of the carrier, we also performed the experiment with 1.6 and 3.2 μm unlabelled particles, obtaining similar results (Figure 5C).

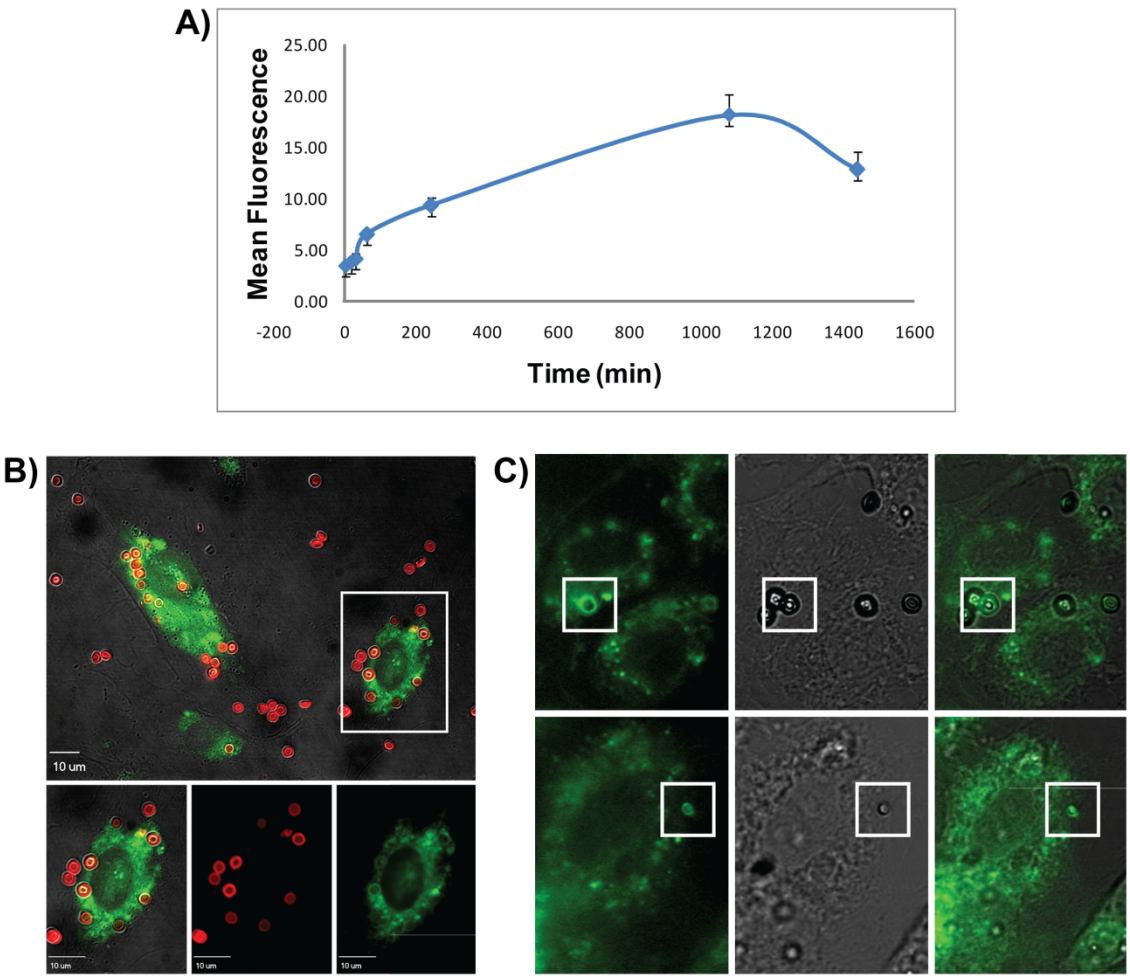

Figure 5 A) Flow cytometry analysis of pH-Rhodo-conjugated particles incubated for up to 24 hours with HMVECs. The cells mean fluorescence is reported over time. B) and C) Confocal images of GFP-NPC1 transfected HMVECs incubated for 4 hours with either dylight 594-conjugated silicon particles B) or un-labeled particle C). The images are presented in merged and separated channels *(Ferrati et al. 'Intracellular trafficking of silicon particles and logic-embedded vectors' Nanoscale 2010, Courtesy of RSCPublishing).*

3.1.3 Intracellular Mobility and Trajectory of S1MPs

In order to further evaluate the effect of size, shape and charge on the intracellualr traffic of the particles we evaluated and compared the trajectory, directionality and rate of migration toward the perinulcear region of different varaiations of carrriers employing real time confocal microscopy. In particular we analyzed 1.6 and 3.2 μm hemispherical porous silicon particles, positively and

negatively charged, as well as three sizes of spherical beads (1, 2.5 and 3 μm). Movies compiled by assembling images taken every 5 minutes for 19 hours over 5 focal planes, were used to manually track particles inside the cells, from the moment they interacted with cell surface until they reached the perinuclear region (Figure 6 A). The two-dimensional time- dipendent coordinates $[x(t),\ y(t)]$ of the particles were used to calculate individual time-averaged mean square displacement (MSDs) employing the following equation:

$$\langle \Delta\, r^2(\tau)\rangle = \langle [x(t+\tau) - x(t)]^2 + \ [y(t+\tau) - y(t)]^2 \rangle$$

Where τ is the 5 minutes time lag between image acquisition.

Once generated, the MSD curves were fitted with the equation: $y = 6Dt^k$ (fitting 1 Figure 6 B). In the specific case of k=1 the equation becomes Fick's law, which describes random, thermally driven diffusion. When $k > 1$ instead, the equation describes the active transport where molecules or particles migrate toward a defined direction. All of the MSD curves were fitted with the equation presenting $k > 1$ which confirmed that the particles were moving inside the cells with an active transport that we previously found to be microtubule mediated. Transport rate for active traffic can be calculated using the following equation: $\langle \Delta\, r^2(\tau)\rangle = 4Dt + v^2t^2$ (Fitting 2 Figure 6 B) where the two terms describe respectively the random diffusion and the active contribution with D the diffusion coefficient and v is the rate of intracellular trafficking. We calculated the rate of perinuclear migration of multiple particle variations obtaining a consistent average rate of 0.5 μm per minute for all samples (Anova test with P=0.005 was used to compare the populations). This result, reported in Figure 6 B in the box charts, suggested that the rate of intracellular migration of the particle-loaded

phagosomes is not influenced, at least in the used range, by the particles size (1.6 and 3.2 μm) the shape (hemispherical and spherical) and the charge (negative and positive).

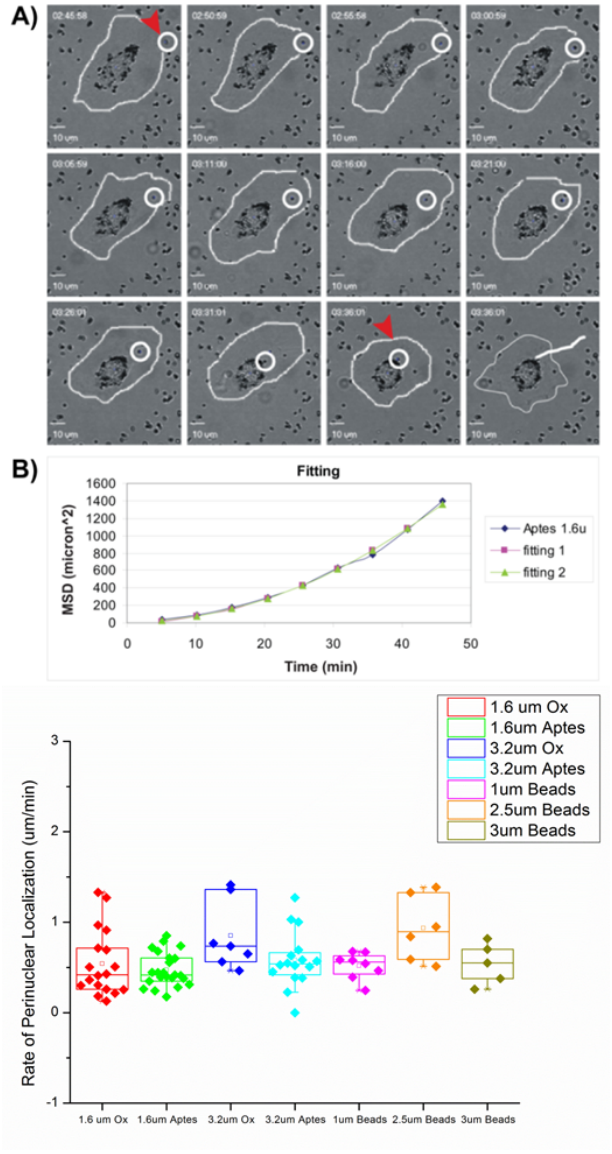

ample
acting
zation.
n). B)
report
micro-
rticles
3 μm)
logic-

3.1.4 Mitotic Trafficking

For biomedical application it is important to understand the impact of particles on cellular events such as the cell cycle. The effect of the particles presence as well as their redistribution during proliferation could potentially introduce disparities and challenges in imaging or treatment of the cells. We therefore investigated the ability of cells containing particles to undergo mitosis by means of real time confocal microscopy, with particular interest on the fate of the particles. Taking images in five focal planes every 5 minutes for 24 hours, we were able to capture the all sequence of events during the mitotic process of HMVECs-bearing particles. The mechanism of endosomes traffic during mitosis involves microtubules, with a centripetal movement of vesicles toward the central region in the first part of the process, and a polarized partitioning along the intercellular bridges toward the end of the process. Mitotic traffic of endosomes-containing particles appear to follow the same mechanism, with the particles accumulating in the central

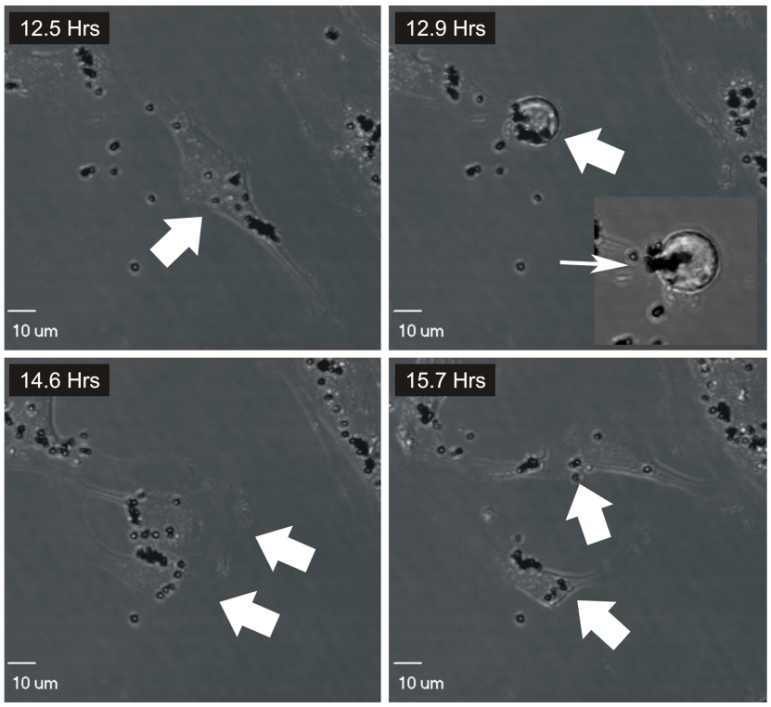

- **Figure 7** Real-time confocal imaging of HMVECs containing 1.6 μm particles undergoing mitosis. The white arrows highlight the initial cell and then the two daughter cells containing equal amounts of microparticles *(Ferrati* and Serda* et al. 'Mitotic trafficking of silicon microparticles' Nanoscale, 2009, Courtesy of RSCPublishing). *shared first authorship.*

region after approximately 30 minutes from the beginning of the process (Figure 7, top right) and then migrating in the two daughter cells a later time points. During this highly ordered process organelles, such as endosomes, are therefore equally divided between two daughter cells. The integrity of the process was found to be unaffected by the presence. Figures 7 and 8 show indeed a time-lapse sequence of images of a cell, containing respectively 1.6 or 3.2 μm particles before the mitotic event, and equally partitioning the particles between the two daughter cells during the cellular division.

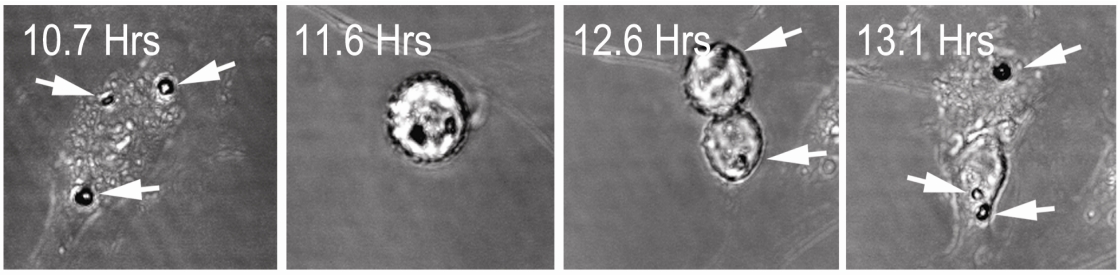

Figure 8 Real-time confocal imaging of HMVECs containing 3.2 μm particles undergoing mitosis. The white arrows highlight the initial cell and then the two daughter cells containing equal amounts of microparticles *(Ferrati* and Serda* et al. 'Mitotic trafficking of silicon microparticles' Nanoscale, 2009, Courtesy of RSCPublishing) *shared first authorship.*

This is consistent with the fact that each S1MP is encapsulated in phagosomes, as we have shown in TEM micrographs, therefore each particle represents an endosome and follows the same fate of the single vesicles during the process. This study confirmed that particles are not compromising cellular function, resulting in compatible and safe use for *in vivo* study. Partitioning of S1MPs showed persistence over longer time points as it was monitored for 6 days by means of fluorescent microscopy. HMVECs were incubated with 3.2 μm fluorescently labeled particles and then sorted

with FACS to assure a homogeneous population of particles-containing cells. Number of particles per cell was manually counted each day using the bright field images to define cell boundaries and fluorescent images to evaluate particle content. Two representative images of days 2 and 6 are reported in Figure 9 A , the particles counts over time are reported as a Box and Whisker Chart (Figure 9 B) where the statistical boxes summarize the 25^{th}, 75^{th},50^{th} percentiles and the average number of particles in the cells is written on top of each box. Significant changes in particles content, based on ANOVA test with P=0.005, were marked with an asterisk and well were correlated with the 48 hours doubling time of HMVECs. Indeed each 48 hours the average number of particles per cell decreases by half, confirming particle partitioning during mitotic events over time, for both 1.6 and 3.2 μm particles.

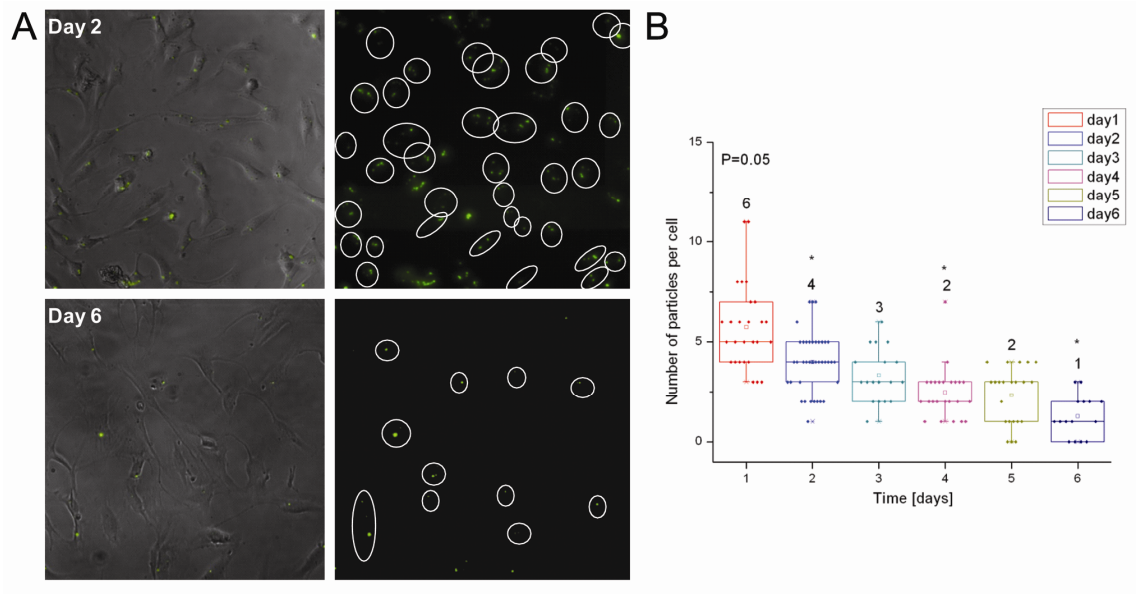

Figure 9 Quantitative analysis of the number of particles per cell during proliferation. FITC-labeled particles were incubated with HMVECs and then a homogenous population of cells with equal number of internalized particles was sorted at FACS based on fluorescence. A) Representative fluorescent images of HMVECs- containing particles at day 2 and 6. B) The number of particles per cells at different time points is represented through statistical box charts. The 25th, 75th (box margins) and 50th (middle line) percentiles and the average number of particle per cell per day (number on top of the box) are reported. Statistically different amounts are marked with a star *(Ferrati* and Serda* et al. 'Mitotic trafficking of silicon microparticles' Nanoscale, 2009, Courtesy of RSCPublishing) *shared first authorship.*

3.1.5 Direct Cell-to-Cell transfer of Silicon Microparticles.

After having analyzed the impact of microparticles on endothelial cell proliferation and mitosis, we investigated the retention of particles within the cells and their possible intercellular transport. Real time confocal microscopy was employed to monitor HMVEC cells incubated with 3.2 μm oxidized silicon particles overnight. Direct cell-to-cell transfer was observed as reported in the time-lapse sequence of

pseudo colored (Figure 10A) and unaltered confocal images (Figure 10B). In the sequence of images a cell (colored in blue, which we called the 'donor cell') containing one particle, transferr it to the neighbor cell (red cell, which we called the 'recipient cell'). The particle's perinuclear localization in the donor cells and its movement associated with the cell migration suggested that the particle is fully internalized by the donor cell. At the moment of transfer the donor and recipient cells align each other and their membranes appear to expand and open to accommodate the particles. The transferred particle appears then to migrate to the perinuclear region of the recipient cell suggesting fully internalization.

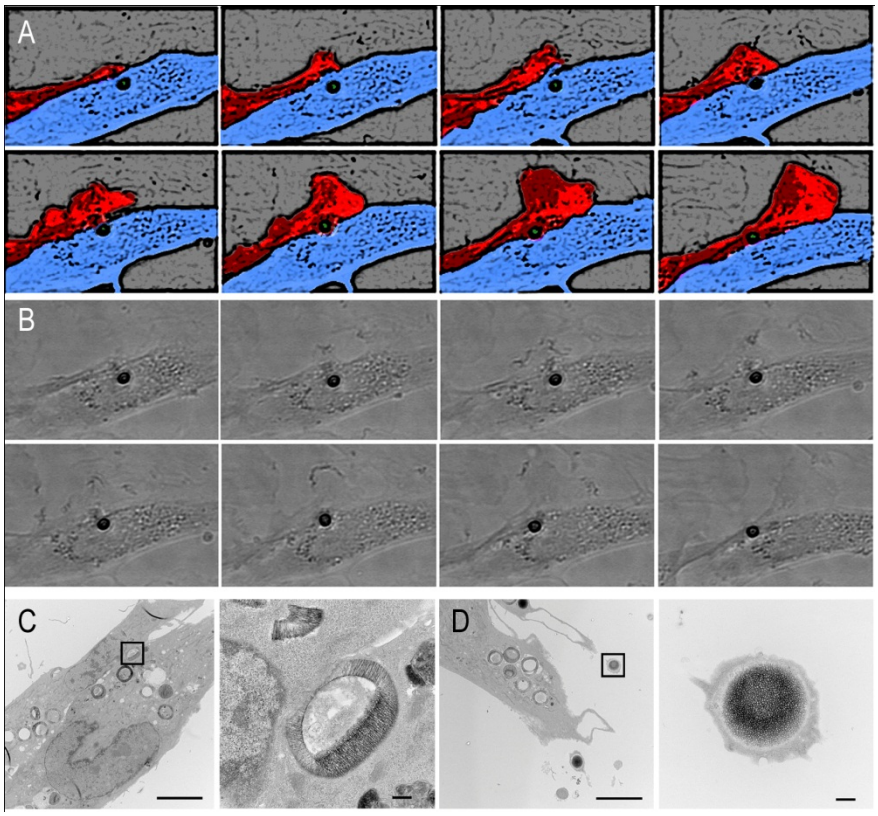

Figure 10 Real-time confocal imaging of HMVECs containing 3.2 μm particles at 37ºC. Transfer of the particle between cells is highlighted by pseudo-coloring the cells: blue the donor cell and red the recipient cell (Top). TEM images of HMVECs incubated

for four hours with 3.2 μm particles. Scale bars are respectively 10 μm, 2 μm and 500nm (Bottom).

TEM micrographs of HMVECs treated for 4 hours with silicon particles (Figure 10 C) show images of adjacent cells containing particles which would support the direct transfer between cells. The particles are indeed near the cells membrane boundaries, where the two membranes appear fused each other suggesting fusion of the two cells. In The TEM images we also observed particles in the area surrounding the cells enclosed in membranes (Figure 10 D), which could potentially be particles secreted by the cells.

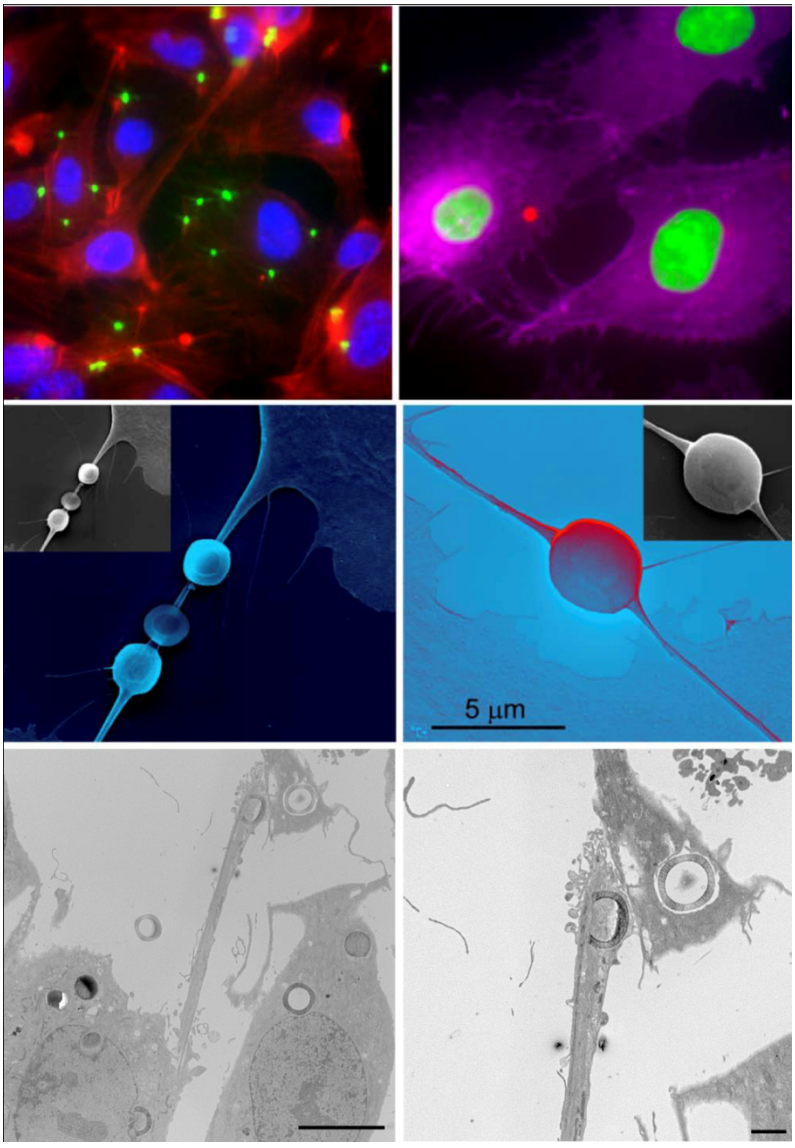

Figure 11 Confocal images (Top) of HMVECs incubated with 3.2 µm particles at 37ºC (5:1 particles/ cells). Cells were stained with Alexa Fluor 555 Phalloidin while the particles are fluorescently labeled. Pseudo-colored SEM images (middle) of HMVECs interacting with 3.2 µm porous silicon particles. TEM micrographs (bottom) of HMVECs incubated with 3.2 µm particles at 37ºC for 4 hours. Pseudopodia containing particles are visible in both SEM and TEM images. (scale bar 10µm and 2µm respectively)

In addition Figure 11 top (Data generated by Dr. Rita Serda) shows confocal images of Alexa fluor Phalloidin stained HMVECs where pseudopodia connecting the cells presenting actin filaments is visible. Similarly elongated cellular structures connecting neighbor cells that also contain silicon particles are visible in SEM (Data generated by Dr. Rita Serda) and TEM images (Figure 11, middle and bottom). These types of pseudopodia are very close in structure to the tunneling-nanotubes (TNTs) which are thin tubular membrane protrusions known to be involved in communication [65], transfer of organelles and long distance connectivity between cells [66]. TNTs have been shown to be exploited by cells for the intercellular transport of nanoparticles. Mi et al.[67] followed the fate of quantum dots micron-aggregates in human hepatocellular carcinoma cells and observed transfer between cells happening through the formation of TNTs, which connected the two cells involved in the process. The particles transported along the TNTs were encapsulated in lysosomes and the whole organelle was transferred between the cells.

Although these results cannot fully explain the transfer mechanism, they can qualitatively describe the process, highlighting the complexity and dynamicity of the interaction of cells with particles.

Moreover Figure 12 reports another time-lapse sequence of confocal images acquired in the same experiment, but in a separate field of view. The images show the transfer of two particles between 2 adjacent cells (pseudo colored in pink and blue) mediated by a small active cell (green cell), which acts as a shuttle. This ‘shuttle cell’ transfers the first particles (Figure 12A) and then goes back to the donor cells (Figure 12B) and picks up another particle. From the sequential images it is possible to see how

the donor cells is extended in the region where the transfer occurs and how the green cell precisely attached to that location and grab the particle.

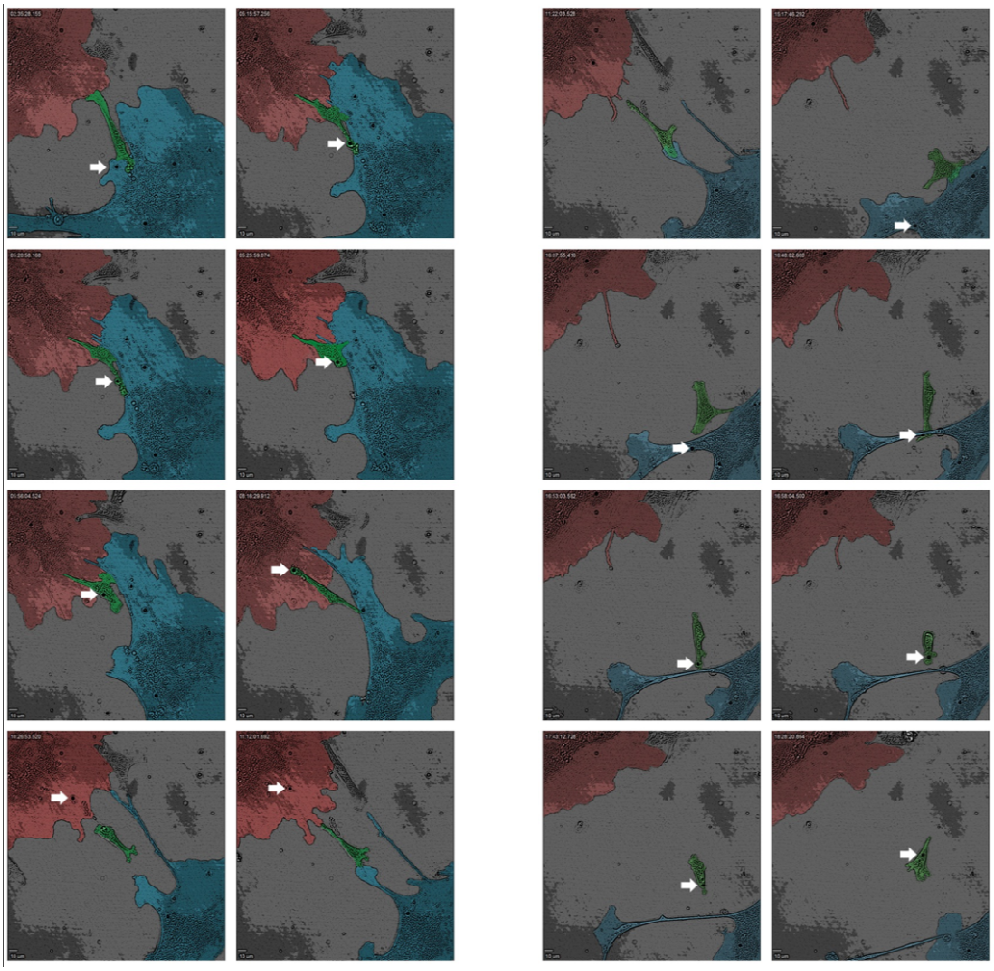

Figure 12 Real-time confocal imaging of HMVECs containing 3.2 μm particles undergoing intercellular transfer. The cells have been pseudo colored to highlight the cellular margins and the white harrow points to the particle involved into the process.

The rate of inter-cellular transfer was also quantified by means of Imagestreaming X System and Ideas software, in collaboration with Dr.Summers and Dr. Rees at the University of Swansea, in UK. Two populations of cells, respectively containing red (Alexa Fluor 555) or green (Alexa Fluor 488)-labelled microparticles, were co-cultured

for 24 hours and dual labeled cells were quantified with the system (Figure 13). The single labeled populations were used as controls to set up the spectral compensation.

When the cells were co-cultured in regular mediun containing serum the exchange after 24 hours was 1% while when the cells were cultured in serum-free media the exchange increased to 5%. This indicates an involvement of serum in the process and the possibility to manipulate the extent of the process.

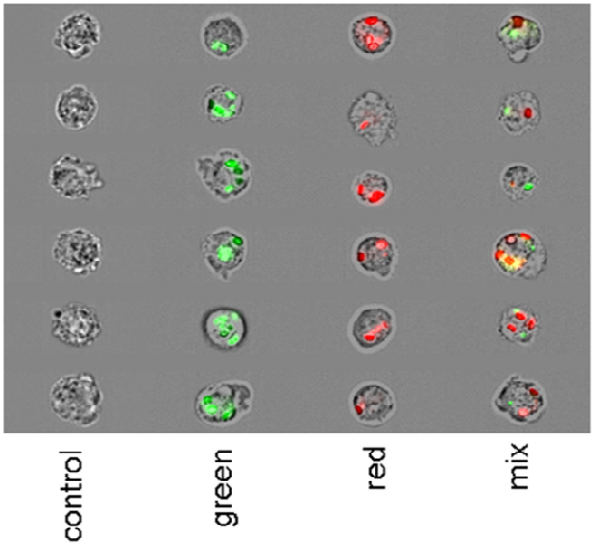

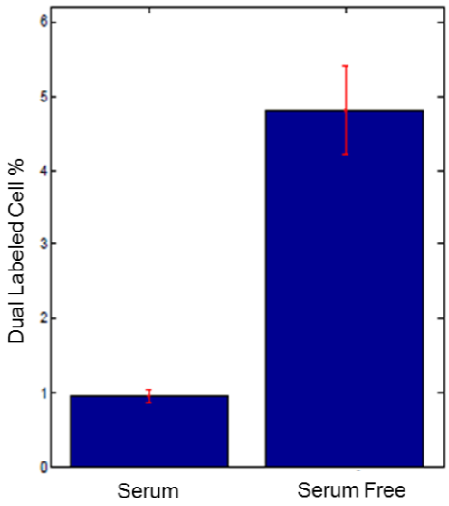

ɔ. HMVEC
wed by co-
ftware were
xchange of
ı was also

This novel phenomenon brings up questions regarding the possibility of achieving long distance communication between cells with transfer of particles. It appears that multiple different mechanisms such as direct cell transfer, TNTs and cell

shuttling could potentially be involved in the transfer of micro-particles between cells bringing additional level of complexity to intra and inter cellular trafficking of particles. In addition the increase in the rate of exchange during serum-starvation may suggest that environmental stress might stimulate the exchange. This could be potentially exploited in tumor environment to rapidly distribute the particles and their payloads between cancer cells.

3.2 Multistage Vectors

3.2.1 Assembly and Characterization

S1MPs were the first components in the assembly of our MSV system serving as carriers for S2NP that can be loaded into the porous structure. The loading procedure was based on capillary suction of the solution containing the S2NP into the pores of the S1MP. The entrapment and retention of the second stage depends on pore size and the electrostatic interactions between the nanoparticles and the porous silicon surface. Both of these parameters can be tuned to achieve the optimal condition for a given S2NP. This allows our system to be very versatile in terms of payloads possibilities.

In order to study the impact of the MSV systems and its intracellular traffic in endothelial cells, we assembled the system loading S1MPs with SPIOs. SPIOs can be used as magnetic resonance imaging (MRI) contrasts agents given their ability to decrease the relation time, T2, when accumulating in a region. They are also employed as hyperthermia agents, targeted drug delivery and cell separation. SPIOs are commercially available in many sizes ranging from a few to hundreds of nanometers in diameter with several different surface coatings such as synthetic polymers and polysaccharides [17]. For the study we employed 15 nm SPIOs coated with amino-polyethylene glycol (PEG) polymer (NH2-PEG SPIOs), since from previous studies [68]

they resulted the best choice in terms of loading capacity into our MSV. The physicochemical characteristics of the nanoparticles were verified employing Zeta Potential analysis and Fourier Transform Infrared (FTIR) - spectroscopy. The particles charge, measured through zeta potential, was checked for NH2-PEG SPIOs and oxidized silicon particles both in phosphate buffer (pH7) and borate buffer (pH5). The NH2-PEG SPIOs net charge were -4mV and +31.2 mV respectively in phosphate (PBS) and borate buffer while oxidized porous silicon particles were respectively -22.5mV and -28mV, showing complementary electrostatic conditions between the two components of our system especially in borate buffer, which was therefore chosen as loading solution for multistage particle assembly. The stability of the SPIOs' coating was tested by incubating the particles for 6 days in PBS (pH 7) and regularly testing the zeta potential in order to confirm the constant value of surface charge of the particles throughout the experiment.

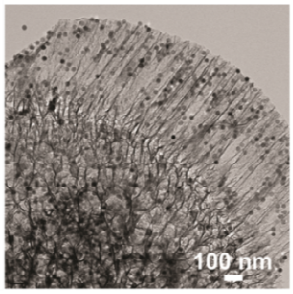

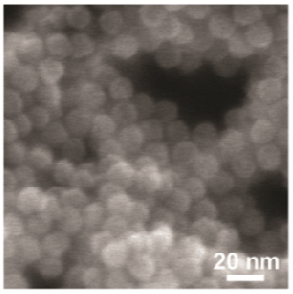

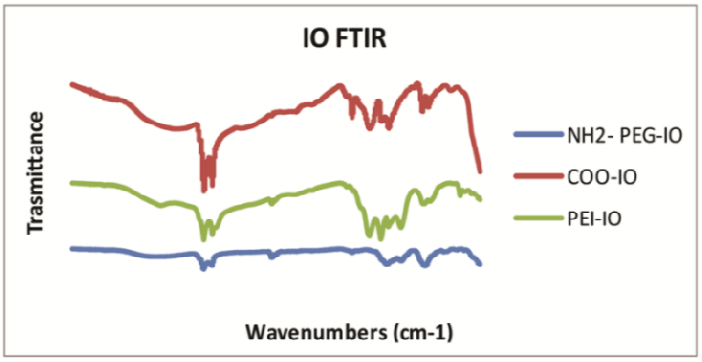

with
ylated
ottom
logic-

FTIR spectroscopy was performed on NH2-PEG SPIOs and compared to carboxylated SPIOs (Figure 14, bottom). NH2-PEG SPIOs spectrum highlighted the presence of the characteristic peaks for primary amines at 3341 cm^{-1} (NH) and 1298 cm^{-1} (CN) and the CH stretching at 2922 -2853 cm^{-1} in addition to the PEG bands presented on both types of particles such as the bands at 1700 cm^{-1} (COOH) and 1104 cm^{-1} (CH_2-OH).

The NH2-PEG SPIOs were loaded through capillary action into 3.2 μm mesopourous discoidal silicon particles and the amount loaded was evaluated by induced coupled plasma optical emission spectroscopy (ICP-OES) resulting in 6.4μg of iron per 3 x 10^6 silicon particles (21% loading efficiency). TEM images, in Figure 14 top, show silicon

particles loaded with the amino-PEG SPIOs, with a detailed zoom on the pores of the particles.

3.2.2 Intracellular Traffic of MSV

The intracellular trafficking of the MSV was studied in HMVECs cells employing TEM microscopy. At early time points (24 and 32 hours) it was possible to image the assembled system internalized in phagosomes into the cells. The SPIOs were still predominantly associated with the carriers although in some phagosomes, regions rich in nanoparticles started to dissociate creating separated vesicles containing SPIOs. In Figure 15 the sequence of events is recapitulated with particular focus on a membrane protrusion budding from the original endosome which will then form a unique vesicle free to independently traffic in the cytoplasm. This suggests an active sorting of the SPIOs from the carriers over time.

We were also interested in understanding the long term fate of the S2NPs. Phenomenon of exocytosis of nanoparticles such as PLGA nanoparticles, carbon nanotubes or SPIOs have been reported in literature.

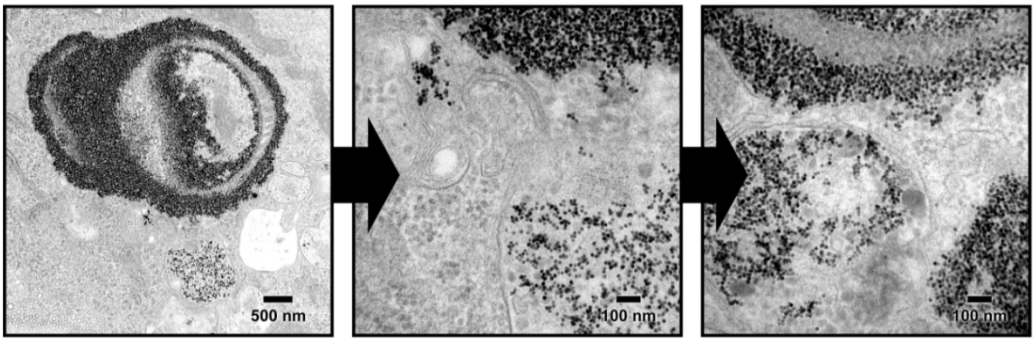

Figure 15 TEM micrographs of multistage system after up take by HMVECs. The system was assembled loading porous silicon microparticles with 15nm amino-PEG SPIOs. Sorting of SPIOs in unique vesicles presenting characteristics of multivesicular bodies is visible overtime *(Ferrati et al. 'Intracellular trafficking of silicon particles and logic-embedded vectors' Nanoscale 2010, Courtesy of RSCPublishing).*

To evaluate possible exocytosis of our nanoparticles from HMVECs, we quantitatively measured the concentration of iron over time in the supernatant of cells incubated with the MSV employing ICP-OES. The data in Figure 16 B is reported as percentage of iron released with respect to the SPIOs effectively delivered. The latter was calculated evaluating the initial amount of iron delivered to the cells and subtracting the amount of free particles still present in the medium at 12 hours, since these particles were not internalized and therefore removed during the washing step. We also normalized the results for the iron presents in untreated cells. The amount of SPIOs released per day was found to be on average 25%. This result was compared to the release of free amino-PEG SPIOs not loaded into the multistage system which was on average lower (around 12%). The difference in secretion could be due to difference in trafficking and sorting of endosomes as well as a difference in absolute values of iron per cells which may impact the cellular secretion itself.

TEM images (Figure 16 A) of MSV incubated in HMVEC cells for 7 days supported the decrease of SPIOs from the primary carrier over time. Together this data suggests an active release of S2NPs from the pores of the silicon particles with potential subsequent exocytosis of SPIOs.

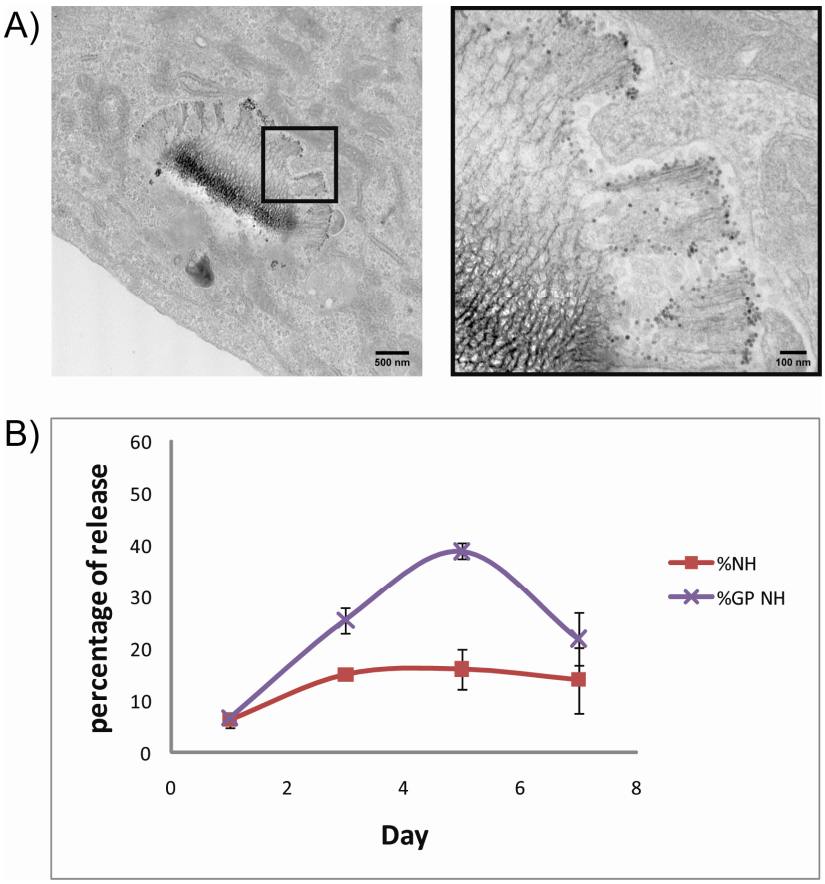

Figure 16 Long term fate of SPIOs loaded into the multistage system. A) TEM image showing the majority of SPIOs been released after 7 days incubation in cells. B) Increase of iron concentration in the medium over time after incubation of multistage (GP-NH) or free SPIOs in HMVECs *(Ferrati et al. 'Intracellular trafficking of silicon particles and logic-embedded vectors' Nanoscale 2010, Courtesy of RSCPublishing).*

3.3 Secreted Biovesicles as Mediator for Intercellular Transfer of Nanoparticles.

The employment of nanoparticles for biomedical applications has brought up questions about their biodistribution in the body and their fate at a cellular level [69]. Our mitotic trafficking data explained particles redistribution during proliferation while the transfer of micro-particles between cells and the preliminary results reporting the increase of iron concentration in the medium over time after treatment of endothelial

cells with our MSV loaded with second stage SPIOs suggested possible secretion of both S1MPs as well S2NPs from cells. For S1MPs we saw that multiple mechanisms were potentially involved into the transfer such as TNTs and direct transfer, we next decided to further investigate the form and mechanism by which S2NPs were instead secreted from HMVECs. For simplicity, we employed free SPIOs as nanoparticles and we characterized their intracellular traffic briefly recapitulating their uptake mechanism in HMVECs and then focusing on their secretion.

3.3.1 Endocytosis of PEI-SPIOs in HMVECs

TEM micrographs (Figure 17 B-D) of HMVECs cells incubated with PEI-SPIOs for 6 hours show the uptake of particles by cells and their localization within endosomes. The encapsulation of the particles in vesicles was also confirmed by confocal microscopy (Figure 17 A). 488-labeled SPIOs were incubated with 594- Wheat Germ Agglutinin (WGA) stained cells. WGA selectively binds to N-acetylglucosamine and N-acetylneuraminic acid thus staining the cellular membrane, which, during the uptake of the particles, forms the endosomes. The co-localizing of particles within the vesicles resulted in a yellow coloration of the endosomes as the sum of the two fluorescent dyes (average overlap coefficient resulted 0.980). Early endosomes are known to be able to mature into late endosomes (also known as multivesicular bodies), which can then fuse with either lysosomes or autophagosomes forming respectively a mature form of lysosomes or hybrid structures such as amphisomes and autolysosomes. Both mature lysosomes and hybrid structures can retain markers of the original organelles, such as: Rab7, LC3 and Lamp1, which are markers for late endosomes, autophagosomes and lysosomes respectively. Therefore any of the markers can be used

to label these organelles. The maturation and fusion between organelles is associated with a movement toward the perinuclear region. From TEM and confocal images, the presence of SPIOs within the endosomes does not seem to affect their maturation and their final co-localization in the perinuclear region.

Moreover, the internalization of the particles did not negatively impact the cells as both their morphology and subcellular structure, such as nuclei and organelles; appear healthy in the TEM micrographs. In addition, the MTT assay (Figure 18 A) confirmed that the cellular proliferation over 4 days of incubation with PEI-SPIOs (2 μg/ml) was not affected.

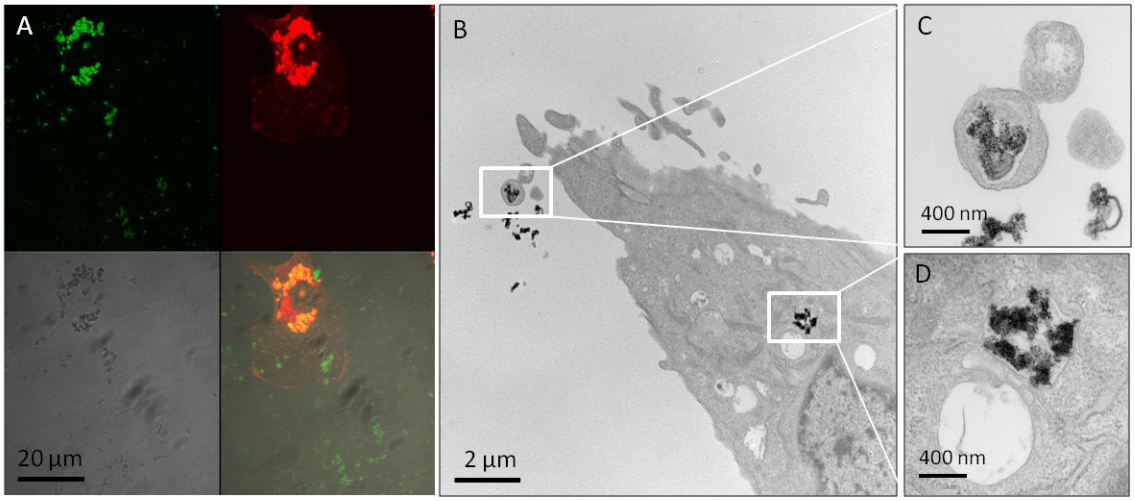

Figure 17 A) Co-localization of 488 Dylight labeled-PEI-SPIOs with 594-WGA-labeled vesicles after overnight incubation in HMVECs. B) TEM micrographs of HMVECs incubated with PEI-SPIOs. Vesicles containing SPIOs are visible inside as well as outside the cell.

3.3.2 Secretion of Microvesicles Containing SPIOs

In our previous set of experiments we hypothesized that the increase of iron concentration in the supernatant was due to the exocytosis of second stage nanoparticles, released from the silicon carrier. In the present study we further

investigated this phenomenon to understand in which form the SPIOs were secreted. The TEM micrograph reported in Figures 17-C, clearly shows that endocytosed-SPIOs can be secreted into the surrounding area by HMVECs encapsulated into biovesicles. Next we analyzed the content of the conditional medium of HMVECs recovered after three days of incubation with PEI-SPIOs. We concentrated the supernatant by centrifugation obtaining a dark pellet (Figure 18 B), which suggested the presence of secreted iron nanoparticles.

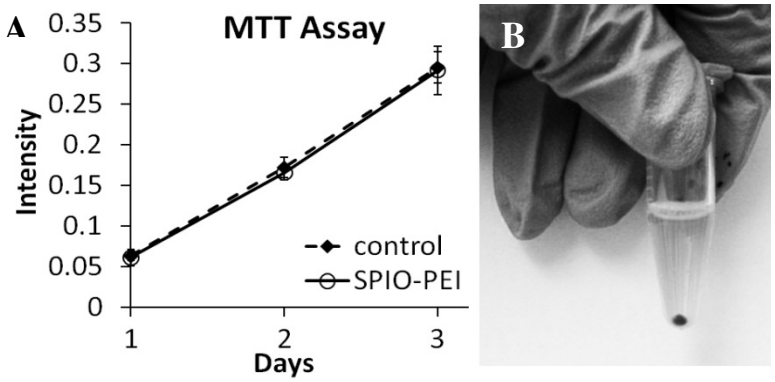

Figure 18 A) MTT proliferation assay of HMVECs incubated with PEI-SPIOs. B) Concentrated conditional medium form HMVECs incubated for 3 days with PEI-SPOIs.

The ultrastructural characterization of the samples by TEM revealed the presence of vesicles containing nanoparticles (Figure 19). The vesicles have an average size of 1μm and from a morphological point of view they present various characteristics of multivesicular bodies (MVB) (Figure 19 A), autophagosomes (Figure 19 C) and primary lysosomes (Figure 19 B) containing recycled membrane bundles, smaller endocytic vesicles, partially degraded ribosomes and rough ER. Next we tested the presence of Lamp1 as a membrane biomarker for the biovesicles.

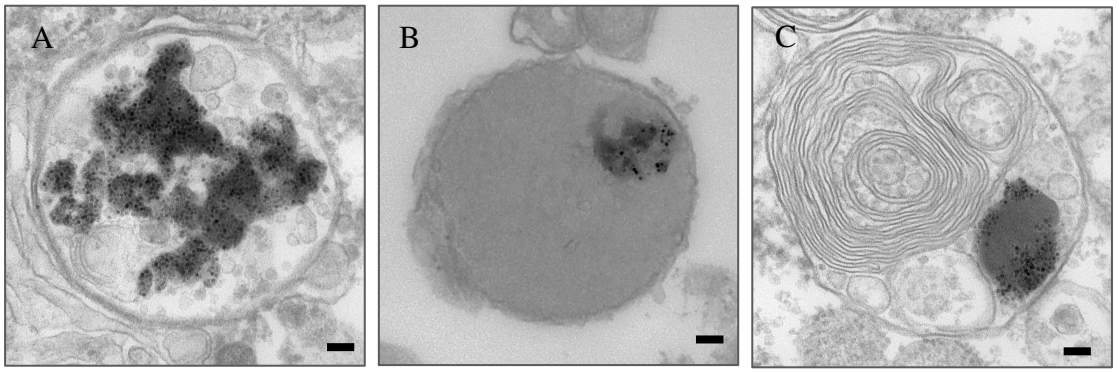

Figure 19 TEM micrographs of concentrated medium form HMVECs incubated with PEI-SPIOs. The ultra-structural analysis revealed presence of secreted microvesicles containing SPIOs.(Scale bar 100 nm)

The concentrated pellet was incubated with a FITC labeled Lamp1 antibody and analyzed with confocal microscopy, using reflectance to visualize the clusters of iron oxide nanoparticles. Biovesicles containing iron nanoparticles appeared to be Lamp1 positive as shown in Figure 21-A, confirming their endosomal origin. In addition it was previously reported that exocytosis depends on the molecular weight of the cargo: lower molecular weight molecules are recycled from early endosomes while higher molecular weight molecules are secreted from larger and slower compartments, presumably lysosomes [70]. Exocytosis of fluid phase markers was therefore faster than the secretion of nanoparticles due to the different size and nature of the cargo [53]. The release of SPIOs appears to be slow and it becomes substantial after 48 hours suggesting release from the slower compartment.

We have schematically outlined in Figure 20 a possible mechanism for the release of vesicle-enclosed nanoparticles from endothelial cells. The first part of the schematic summarizes the well-established cellular uptake of nanoparticles through

endocytosis, while the second part describes the rerouting of mature endocytic vesicles-containing nanoparticles and their release outside the cell.

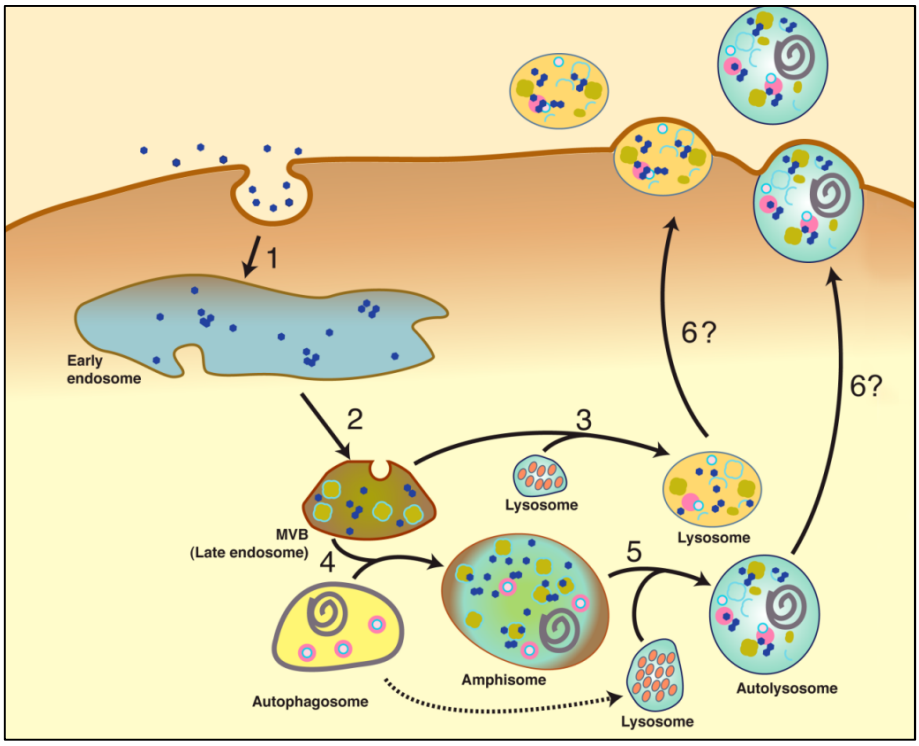

Figure 20 Schematic of proposed mechanism of secretion of microvesicles containing nanoparticles. The SPIOs enter in the cells via endocytosis trafficking and therefore they traffic to early endosomes (1). From there, the vesicles containing SPIOs mature in late endosomes or multivesicular bodies (MVB) (2) and then finally fuse to either lysosomes (3) or auotphagosomes (4) to create respectively lysosomes and autolysosomes. These matured vesicles could then be secreted outside the cell as whole structures (6).

This hypothesis is supported by previous knowledge of similar mechanisms in endothelial cells. These cells are naturally programmed to control the passage of fluids and molecules through vessel walls and one of the mechanisms they exploit is transcytosis. During this process they internalize cargos from the lumen side and subsequently release it in the interstitial space; an example is the GP60 receptor-mediated transcellular transport of albumin across the endothelium [71]. Therefore vascular cells present the machinery to perform exocytosis. Vascular endothelial growth factor (VEGF)-activated endothelial cells [72] have also recently been shown to release specialized granules, called Weibed-Palade bodies (WPb), which are up to 3 μm in length and 0.1-0.2 μm in width [73], comparable with our vesicle size.

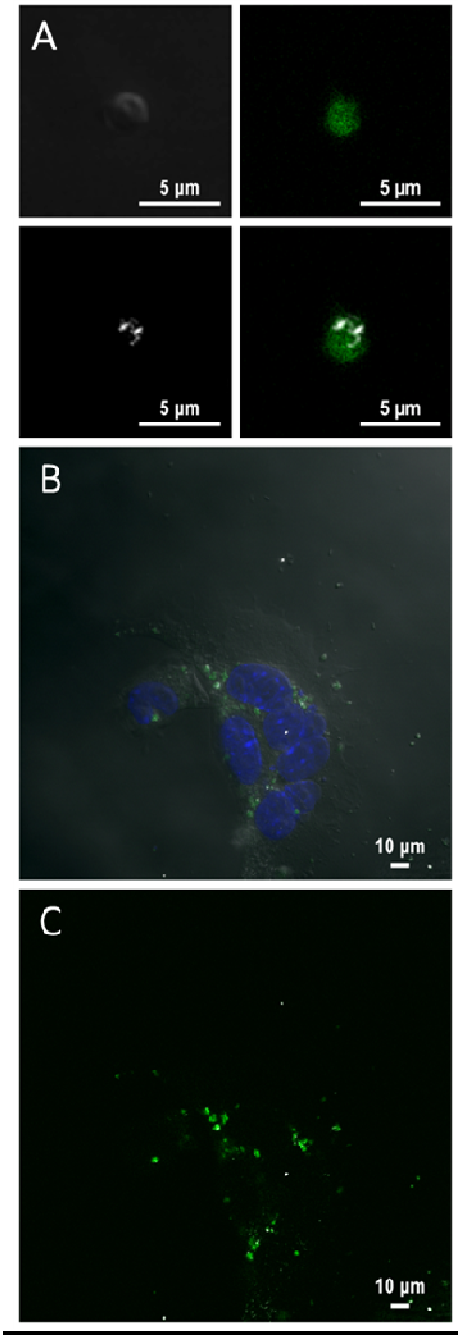

esicles,
Lamp1
T1 are

3.3.3 Intercellular Transfer of Nanoparticles through Microvesicles.

In order to test if endothelial cell derived microvesicles could be involved in the inter-cellular transfer of nanoparticles, Lamp1-FITC labeled microvesicles were incubated with 4T1 breast cancer cells for 24 hours. Confocal microscopy of the treated cells (Figure 21, B-C) revealed an association of the FITC-vesicles with the cancer cells. The presence of SPIOs clusters within the green vesicles was detected by reflectance while the cell morphology was assessed by staining the nuclei with DAPI and visualizing the cell borders with bright field. To confirm microvesicle uptake by recipient cells we also performed TEM imaging on three different cell lines incubated overnight with the concentrated pellet secreted by endothelial cells (Figure 22). HMVECs (Figure 22-A) cells as well as two breast cancer cell lines, MCF7 and 4T1 (respectively Figure 22 B and C), were employed for the experiment. From the TEM micrographs we can clearly see the presence of iron oxide nanoparticles confined in vesicles within the recipient cells.

Together the confocal and TEM data suggest the uptake of the cell-released microvesicles containing SPIOs by recipient cells and therefore their possible role as a mediator of nanoparticles transport between different cells. The process is complex and dynamic as the vesicles can be re-internalized by other endothelial cells or by different types of cells, such as cancer cells. Similar results were obtained by Luciani et al. [54c], although their study was limited to macrophages as donor and recipient cells. Our data therefore extends the study to a wider range of cells suggesting a more ubiquitous presence of this process. Given their bio-genesis, the use of these microvesicles as carriers for nanoparticles would provide additional advantages in term of compatibility,

cellular uptake and trafficking, as compared to synthetic biovesicles, such as magnetoliposomes, which have already shown to enhance the contrast agent properties of SPIOs due to their confinement [74].

From a broader point of view, since the vasculature represents a biological barrier *in vivo* for i.v. injected drug carriers, which has to be overcome in order to reach the lesion site [20b 29, 75], we therefore propose that the biological vesicles could be exploited to allow nanoparticles to cross the endothelial barrier and transfer particles and drugs to tumor cells. Although further studies are necessary to fully characterize the pathway, we can speculate that in the tumor environment, where VEGF concentration is high, secretion of biovesicles could be potentially more prevalent, as shown for WPb, leading to substantial release of microvesicles containing S2NPs.

This finding expands our previous data reporting evidence of exocytosis of nanoparticles from HMVECs upon treatment with a MSVs loaded with amino-PEG SPIOs [64]. The hypothesized mechanism of secretion could give insights into the long term fate of the unique vesicles that were budding overtime from the endosome encapsulating the silicon carrier. The novel vesicles were shown to independently traffic in the cells and they could potentially be secreted as a whole structure explaining the increase of iron in the supernatant.

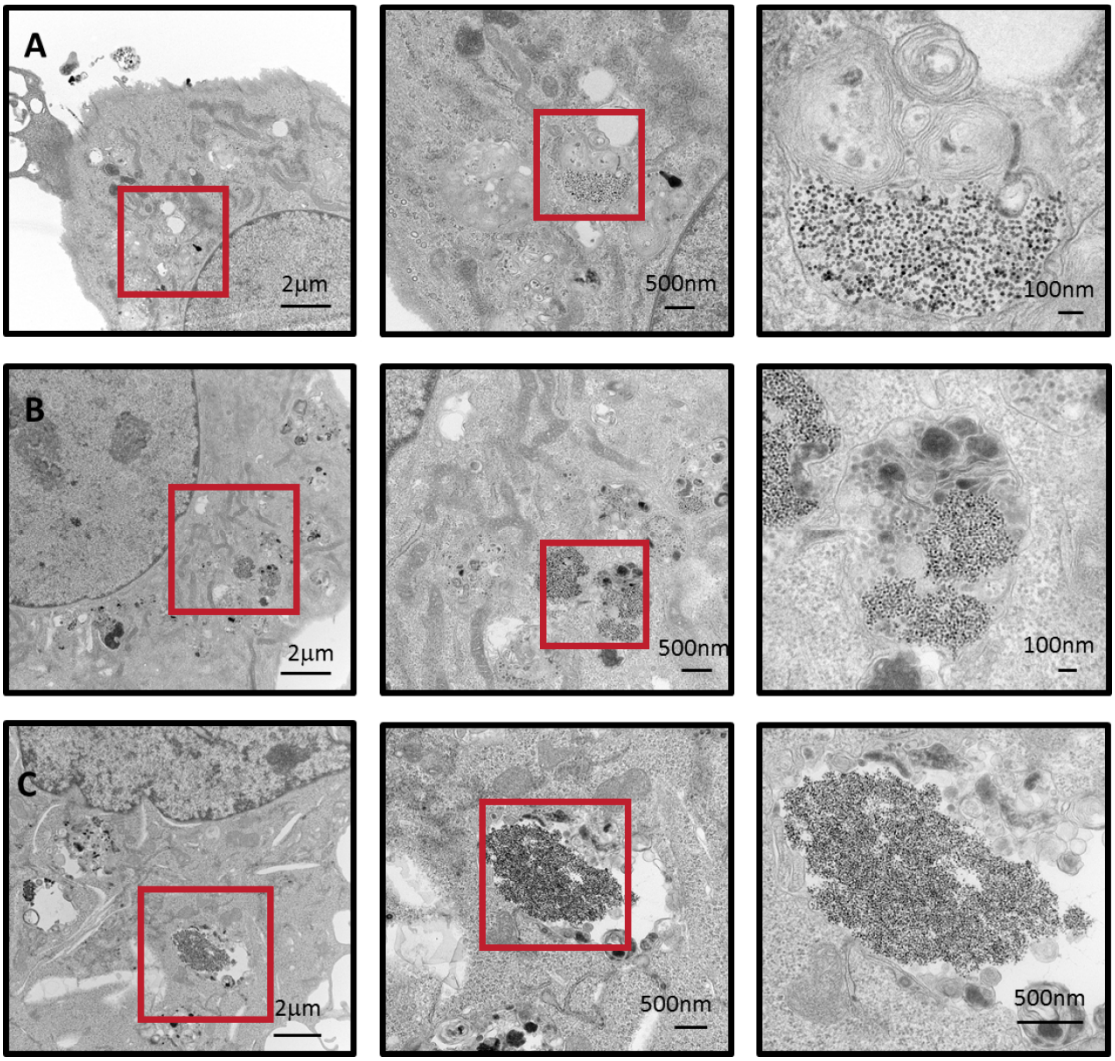

Figure 22 TEM micrographs of recipient cells. A) HMVECs B) MCF7 C) 4T1 incubated overnight with secreted microvesicles. In each line represent consecutive zooms highlighting the presence of iron oxide nanoparticles in the up taken vesicles.

4 Conclusions

In summary, in this work we investigated the cellular trafficking of our multistage drug delivery system, assembled by loading porous silicon microparticles with super-paramagnetic iron oxide nanoparticles, in endothelial cells.

The first part of the study was focused on the understanding of the intracellular localization and migration properties of the silicon carriers. We demonstrate that the regardless the size (1.6 or 3.2 μm) or the surface functionalization (APTES vs oxidized) the silicon carriers are internalized by endothelial cells through phagocytosis and end up in the cells encapsulated in vesicles (phagosomes). These phagosomes are able to mature and move toward the perinuclear region through an active-microtubule-mediated mechanism. The rate of migration for different variations of microparticles was characterized and no impact on the microparticle size, charge and shape was observed. We also studied the long-termfate of the particles with respect to cell proliferation and intercellular transfer, highlighting particle partitioning between daughter cells as well as intercellular transfer.

The second part of the study was instead focused on the loading of the multistage system with second stage nanoparticles (SPIOs) and investigating the intracellular fate of the SPIOs once the MSVs were internalized in HMVECs. As expected, once internalized in the cells, MSVs were encapsulated in phagosomes, but the SPIOs were released over time from the pores and were sorted into unique vesicles (most likely multi-vesicular bodies) which were able to independently traffic inside the cells. Quantitative increase of iron over time in the supernatant suggested the possibility of iron oxide exocytosis.

This hypothesis was further investigated in the third and last part of the work where, through ultra-structural analysis of the conditional medium of HMVECs incubated with SPIOs, it was possible to identify endothelial-cell secreted biovesicles containing iron oxide nanoparticles. The morphology and dimension suggest that these microvesicles are lysosomal in origin with combined features of multivesicular bodies and autophagosomes. This result supports the possibility of a more ubiquitous presence of the release of microvesicles among cells which are not part of the phagocytic immunosystem and provides further insights into the long term fate of nanoparticles in cells. These microvesicles can also mediate the transfer of SPIOs between cells, not only between endothelial cells but also between cancer cells, we therefore propose that the biological event of intercellular transfer of nanoparticles within vesicles could be exploited to allow nanoparticles to cross the endothelial barrier and provide signals or therapeutics to tumor cells.

5 Bibliography

1. Theis, T.; Parr, D.; Binks, P.; Ying, J.; Drexler, K. E.; Schepers, E.; Mullis, K.; Bai, C.; Boland, J. J.; Langer, R.; Dobson, P.; Rao, C. N.; Ferrari, M., nan'o.tech.nol'o.gy n. *Nat Nanotechnol* **2006,** *1* (1), 8-10.

2. (a) Blanco, E.; Hsiao, A.; Mann, A. P.; Landry, M. G.; Meric-Bernstam, F.; Ferrari, M., Nanomedicine in cancer therapy: innovative trends and prospects. *Cancer Sci* **2011,** *102* (7), 1247-52; (b) Bharali, D. J.; Khalil, M.; Gurbuz, M.; Simone, T. M.; Mousa, S. A., Nanoparticles and cancer therapy: a concise review with emphasis on dendrimers. *Int J Nanomedicine* **2009,** *4*, 1-7; (c) Ferrari, M., Cancer nanotechnology: opportunities and challenges. *Nat Rev Cancer* **2005,** *5* (3), 161-71.

3. Liu, Y.; Miyoshi, H.; Nakamura, M., Nanomedicine for drug delivery and imaging: a promising avenue for cancer therapy and diagnosis using targeted functional nanoparticles. *Int J Cancer* **2007,** *120* (12), 2527-37.

4. Seigneuric, R.; Markey, L.; Nuyten, D. S.; Dubernet, C.; Evelo, C. T.; Finot, E.; Garrido, C., From nanotechnology to nanomedicine: applications to cancer research. *Curr Mol Med* **2010,** *10* (7), 640-52.

5. (a) Choi, H. S.; Liu, W.; Liu, F.; Nasr, K.; Misra, P.; Bawendi, M. G.; Frangioni, J. V., Design considerations for tumour-targeted nanoparticles. *Nat Nanotechnol* **2010,** *5* (1), 42-7; (b) Farokhzad, O. C.; Cheng, J.; Teply, B. A.; Sherifi, I.; Jon, S.; Kantoff, P. W.; Richie, J. P.; Langer, R., Targeted nanoparticle-aptamer bioconjugates for cancer chemotherapy in vivo. *Proc Natl Acad Sci U S A* **2006,** *103* (16), 6315-20.

6. Ding, B. S.; Dziubla, T.; Shuvaev, V. V.; Muro, S.; Muzykantov, V. R., Advanced drug delivery systems that target the vascular endothelium. *Mol Interv* **2006,** *6* (2), 98-112.

7. Anton, K.; Glod, J., Targeting the tumor stroma in cancer therapy. *Curr Pharm Biotechnol* **2009,** *10* (2), 185-91.

8. Hilgenbrink, A. R.; Low, P. S., Folate receptor-mediated drug targeting: from therapeutics to diagnostics. *J Pharm Sci* **2005,** *94* (10), 2135-46.

9. (a) Sugahara, K. N.; Teesalu, T.; Karmali, P. P.; Kotamraju, V. R.; Agemy, L.; Greenwald, D. R.; Ruoslahti, E., Coadministration of a tumor-penetrating peptide enhances the efficacy of cancer drugs. *Science* **2010,** *328* (5981), 1031-5; (b) Ruoslahti, E.; Bhatia, S. N.; Sailor, M. J., Targeting of drugs and nanoparticles to tumors. *J Cell Biol* **2010,** *188* (6), 759-68.

10. Gabizon, A. A., Pegylated liposomal doxorubicin: metamorphosis of an old drug into a new form of chemotherapy. *Cancer Invest* **2001,** *19* (4), 424-36.

11. Desai, N.; Trieu, V.; Yao, Z.; Louie, L.; Ci, S.; Yang, A.; Tao, C.; De, T.; Beals, B.; Dykes, D.; Noker, P.; Yao, R.; Labao, E.; Hawkins, M.; Soon-Shiong, P., Increased antitumor activity, intratumor paclitaxel concentrations, and endothelial cell transport of cremophor-free, albumin-bound paclitaxel, ABI-007, compared with cremophor-based paclitaxel. *Clin Cancer Res* **2006,** *12* (4), 1317-24.

12. Harris, T. J.; Green, J. J.; Fung, P. W.; Langer, R.; Anderson, D. G.; Bhatia, S. N., Tissue-specific gene delivery via nanoparticle coating. *Biomaterials* **2010,** *31* (5), 998-1006.

13. Li, S. D.; Chen, Y. C.; Hackett, M. J.; Huang, L., Tumor-targeted delivery of siRNA by self-assembled nanoparticles. *Mol Ther* **2008,** *16* (1), 163-9.

14. Patil, Y.; Panyam, J., Polymeric nanoparticles for siRNA delivery and gene silencing. *Int J Pharm* **2009,** *367* (1-2), 195-203.

15. Davis, M. E.; Zuckerman, J. E.; Choi, C. H.; Seligson, D.; Tolcher, A.; Alabi, C. A.; Yen, Y.; Heidel, J. D.; Ribas, A., Evidence of RNAi in humans from systemically administered siRNA via targeted nanoparticles. *Nature* **2010,** *464* (7291), 1067-70.

16. Pinaud, F.; Michalet, X.; Bentolila, L. A.; Tsay, J. M.; Doose, S.; Li, J. J.; Iyer, G.; Weiss, S., Advances in fluorescence imaging with quantum dot bio-probes. *Biomaterials* **2006,** *27* (9), 1679-87.

17. Tong, S.; Hou, S.; Zheng, Z.; Zhou, J.; Bao, G., Coating optimization of superparamagnetic iron oxide nanoparticles for high T2 relaxivity. *Nano Lett* **2010,** *10* (11), 4607-13.

18. Jain, T. K.; Reddy, M. K.; Morales, M. A.; Leslie-Pelecky, D. L.; Labhasetwar, V., Biodistribution, clearance, and biocompatibility of iron oxide magnetic nanoparticles in rats. *Mol Pharm* **2008,** *5* (2), 316-27.

19. Thorek, D. L.; Chen, A. K.; Czupryna, J.; Tsourkas, A., Superparamagnetic iron oxide nanoparticle probes for molecular imaging. *Ann Biomed Eng* **2006,** *34* (1), 23-38.

20. (a) Au, J. L.; Jang, S. H.; Zheng, J.; Chen, C. T.; Song, S.; Hu, L.; Wientjes, M. G., Determinants of drug delivery and transport to solid tumors. *J Control Release* **2001,** *74* (1-3), 31-46; (b) Ferrari, M., Frontiers in cancer nanomedicine: directing mass transport through biological barriers. *Trends Biotechnol* **2010,** *28* (4), 181-188.

21. Nie, S., Understanding and overcoming major barriers in cancer nanomedicine. *Nanomedicine (Lond)* **2010,** *5* (4), 523-8.

22. (a) Mehta, D.; Malik, A. B., Signaling mechanisms regulating endothelial permeability. *Physiol Rev* **2006,** *86* (1), 279-367; (b) Michel, C. C.; Curry, F. E., Microvascular permeability. *Physiol Rev* **1999,** *79* (3), 703-61.

23. Corada, M.; Mariotti, M.; Thurston, G.; Smith, K.; Kunkel, R.; Brockhaus, M.; Lampugnani, M. G.; Martin-Padura, I.; Stoppacciaro, A.; Ruco, L.; McDonald, D. M.; Ward, P. A.; Dejana, E., Vascular endothelial-cadherin is an important determinant of microvascular integrity in vivo. *Proc Natl Acad Sci U S A* **1999,** *96* (17), 9815-20.

24. Brightman, M. W.; Reese, T. S., Junctions between intimately apposed cell membranes in the vertebrate brain. *J Cell Biol* **1969,** *40* (3), 648-77; (b) Reese, T. S.; Karnovsky, M. J., Fine structural localization of a blood-brain barrier to exogenous peroxidase. *J Cell Biol* **1967,** *34* (1), 207-17.

25. Takakura, Y.; Mahato, R. I.; Hashida, M., Extravasation of macromolecules. *Adv Drug Deliv Rev* **1998,** *34* (1), 93-108.

26. Di Paolo, A.; Bocci, G., Drug distribution in tumors: mechanisms, role in drug resistance, and methods for modification. *Curr Oncol Rep* **2007,** *9* (2), 109-14.

27. (a) Minchinton, A. I.; Tannock, I. F., Drug penetration in solid tumours. *Nat Rev Cancer* **2006,** *6* (8), 583-92; (b) Maeda, H.; Wu, J.; Sawa, T.; Matsumura, Y.; Hori, K., Tumor vascular permeability and the EPR effect in macromolecular therapeutics: a review. *J Control Release* **2000,** *65* (1-2), 271-84; (c) Cairns, R.; Papandreou, I.; Denko, N., Overcoming physiologic barriers to cancer treatment by molecularly targeting the tumor microenvironment. *Mol Cancer Res* **2006,** *4* (2), 61-70.

28. (a) Hobbs, S. K.; Monsky, W. L.; Yuan, F.; Roberts, W. G.; Griffith, L.; Torchilin, V. P.; Jain, R. K., Regulation of transport pathways in tumor vessels: role of tumor type and microenvironment. *Proc Natl Acad Sci U S A* **1998,** *95* (8), 4607-12; (b) Iyer, A. K.; Khaled, G.; Fang, J.; Maeda, H., Exploiting the enhanced permeability and retention effect for tumor targeting. *Drug Discov Today* **2006,** *11* (17-18), 812-8; (c) Batist, G.; Ramakrishnan, G.; Rao, C. S.; Chandrasekharan, A.; Gutheil, J.; Guthrie, T.; Shah, P.; Khojasteh, A.; Nair, M. K.; Hoelzer, K.; Tkaczuk, K.; Park, Y. C.; Lee, L. W., Reduced cardiotoxicity and preserved antitumor efficacy of liposome-encapsulated doxorubicin and cyclophosphamide compared with conventional doxorubicin and cyclophosphamide in a randomized, multicenter trial of metastatic breast cancer. *J Clin Oncol* **2001,** *19* (5), 1444-54.

29. Wang, Z.; Tiruppathi, C.; Cho, J.; Minshall, R. D.; Malik, A. B., Delivery of nanoparticle: complexed drugs across the vascular endothelial barrier via caveolae. *IUBMB Life* **2011,** *63* (8), 659-67.

30. (a) Chen, K.; Chen, X., Integrin targeted delivery of chemotherapeutics. *Theranostics* **2011,** *1*, 189-200; (b) Xiong, X. B.; Mahmud, A.; Uludag, H.; Lavasanifar, A., Multifunctional polymeric micelles for enhanced intracellular delivery of doxorubicin to metastatic cancer cells. *Pharm Res* **2008,** *25* (11), 2555-66.

31. Tannock, I. F.; Lee, C. M.; Tunggal, J. K.; Cowan, D. S.; Egorin, M. J., Limited penetration of anticancer drugs through tumor tissue: a potential cause of resistance of solid tumors to chemotherapy. *Clin Cancer Res* **2002,** *8* (3), 878-84.

32. Netti, P. A.; Berk, D. A.; Swartz, M. A.; Grodzinsky, A. J.; Jain, R. K., Role of extracellular matrix assembly in interstitial transport in solid tumors. *Cancer Res* **2000,** *60* (9), 2497-503.

33. Jain, R. K., Transport of molecules across tumor vasculature. *Cancer Metastasis Rev* **1987,** *6* (4), 559-93.

34. Ribatti, D.; Mangialardi, G.; Vacca, A., Stephen Paget and the 'seed and soil' theory of metastatic dissemination. *Clin Exp Med* **2006,** *6* (4), 145-9.

35. Pollard, J. W., Tumour-educated macrophages promote tumour progression and metastasis. *Nat Rev Cancer* **2004,** *4* (1), 71-8.

36. Masamune, A.; Kikuta, K.; Watanabe, T.; Satoh, K.; Hirota, M.; Shimosegawa, T., Hypoxia stimulates pancreatic stellate cells to induce fibrosis and angiogenesis in pancreatic cancer. *Am J Physiol Gastrointest Liver Physiol* **2008,** *295* (4), G709-17.

37. Ferrara, N.; Kerbel, R. S., Angiogenesis as a therapeutic target. *Nature* **2005,** *438* (7070), 967-74.

38. (a) Biswas, S.; Criswell, T. L.; Wang, S. E.; Arteaga, C. L., Inhibition of transforming growth factor-beta signaling in human cancer: targeting a tumor suppressor network as a therapeutic strategy. *Clin Cancer Res* **2006,** *12* (14 Pt 1), 4142-6; (b) Arteaga, C. L.; Hurd, S. D.; Winnier, A. R.; Johnson, M. D.; Fendly, B. M.; Forbes, J. T., Anti-transforming growth factor (TGF)-beta antibodies inhibit breast cancer cell tumorigenicity and increase mouse spleen natural killer cell activity. Implications for a possible role of tumor cell/host TGF-beta interactions in human breast cancer progression. *J Clin Invest* **1993,** *92* (6), 2569-76; (c) Peng, S. B.; Yan, L.; Xia, X.; Watkins, S. A.; Brooks, H. B.; Beight, D.; Herron, D. K.; Jones, M. L.; Lampe,

J. W.; McMillen, W. T.; Mort, N.; Sawyer, J. S.; Yingling, J. M., Kinetic characterization of novel pyrazole TGF-beta receptor I kinase inhibitors and their blockade of the epithelial-mesenchymal transition. *Biochemistry* **2005,** *44* (7), 2293-304.

39. Petros, R. A.; DeSimone, J. M., Strategies in the design of nanoparticles for therapeutic applications. *Nat Rev Drug Discov* **2010,** *9* (8), 615-27.

40. Rejman, J.; Oberle, V.; Zuhorn, I. S.; Hoekstra, D., Size-dependent internalization of particles via the pathways of clathrin- and caveolae-mediated endocytosis. *Biochem J* **2004,** *377* (Pt 1), 159-69.

41. Bareford, L. M.; Swaan, P. W., Endocytic mechanisms for targeted drug delivery. *Adv Drug Deliv Rev* **2007,** *59* (8), 748-58.

42. Mitragotri, S., In drug delivery, shape does matter. *Pharm Res* **2009,** *26* (1), 232-4.

43. Decuzzi, P.; Ferrari, M., Design maps for nanoparticles targeting the diseased microvasculature. *Biomaterials* **2008,** *29* (3), 377-84.

44. Pasqualini, R.; Ruoslahti, E., Organ targeting in vivo using phage display peptide libraries. *Nature* **1996,** *380* (6572), 364-6.

45. Kakar, S. S.; Jin, H.; Hong, B.; Eaton, J. W.; Kang, K. A., LHRH receptor targeted therapy for breast cancer. *Adv Exp Med Biol* **2008,** *614*, 285-96.

46. Olson, W. C.; Heston, W. D.; Rajasekaran, A. K., Clinical trials of cancer therapies targeting prostate-specific membrane antigen. *Rev Recent Clin Trials* **2007,** *2* (3), 182-90.

47. Kularatne, S. A.; Wang, K.; Santhapuram, H. K.; Low, P. S., Prostate-specific membrane antigen targeted imaging and therapy of prostate cancer using a PSMA inhibitor as a homing ligand. *Mol Pharm* **2009,** *6* (3), 780-9.

48. Dharap, S. S.; Wang, Y.; Chandna, P.; Khandare, J. J.; Qiu, B.; Gunaseelan, S.; Sinko, P. J.; Stein, S.; Farmanfarmaian, A.; Minko, T., Tumor-specific targeting of an anticancer drug delivery system by LHRH peptide. *Proc Natl Acad Sci U S A* **2005,** *102* (36), 12962-7.

49. Dhar, S.; Gu, F. X.; Langer, R.; Farokhzad, O. C.; Lippard, S. J., Targeted delivery of cisplatin to prostate cancer cells by aptamer functionalized Pt(IV) prodrug-PLGA-PEG nanoparticles. *Proc Natl Acad Sci U S A* **2008,** *105* (45), 17356-61.

50. Gruenberg, J., The endocytic pathway: a mosaic of domains. *Nat Rev Mol Cell Biol* **2001,** *2* (10), 721-30.

51. Thery, C.; Zitvogel, L.; Amigorena, S., Exosomes: composition, biogenesis and function. *Nat Rev Immunol* **2002,** *2* (8), 569-79.

52. Beyer, C.; Pisetsky, D. S., The role of microparticles in the pathogenesis of rheumatic diseases. *Nat Rev Rheumatol* **2010,** *6* (1), 21-9.

53. Panyam, J.; Labhasetwar, V., Dynamics of endocytosis and exocytosis of poly(D,L-lactide-co-glycolide) nanoparticles in vascular smooth muscle cells. *Pharm Res* **2003,** *20* (2), 212-20.

54. (a) Serda, R. E.; Mack, A.; van de Ven, A. L.; Ferrati, S.; Dunner, K., Jr.; Godin, B.; Chiappini, C.; Landry, M.; Brousseau, L.; Liu, X.; Bean, A. J.; Ferrari, M., Logic-embedded vectors for intracellular partitioning, endosomal escape, and exocytosis of nanoparticles. *Small* **2010,** *6* (23), 2691-700; (b) Kustermann, E.; Himmelreich, U.;

Kandal, K.; Geelen, T.; Ketkar, A.; Wiedermann, D.; Strecker, C.; Esser, J.; Arnhold, S.; Hoehn, M., Efficient stem cell labeling for MRI studies. *Contrast Media Mol Imaging* **2008,** *3* (1), 27-37; (c) Luciani, N.; Wilhelm, C.; Gazeau, F., The role of cell-released microvesicles in the intercellular transfer of magnetic nanoparticles in the monocyte/macrophage system. *Biomaterials* **2010,** *31* (27), 7061-9.

55. Jin, H.; Heller, D. A.; Strano, M. S., Single-particle tracking of endocytosis and exocytosis of single-walled carbon nanotubes in NIH-3T3 cells. *Nano Lett* **2008,** *8* (6), 1577-85.

56. Wilhelm, C.; Lavialle, F.; Pechoux, C.; Tatischeff, I.; Gazeau, F., Intracellular trafficking of magnetic nanoparticles to design multifunctional biovesicles. *Small* **2008,** *4* (5), 577-82.

57. Tasciotti, E.; Liu, X.; Bhavane, R.; Plant, K.; Leonard, A. D.; Price, B. K.; Cheng, M. M.; Decuzzi, P.; Tour, J. M.; Robertson, F.; Ferrari, M., Mesoporous silicon particles as a multistage delivery system for imaging and therapeutic applications. *Nat Nanotechnol* **2008,** *3* (3), 151-7.

58. (a) Godin, B.; Tasciotti, E.; Liu, X.; Serda, R. E.; Ferrari, M., Multistage nanovectors: from concept to novel imaging contrast agents and therapeutics. *Acc Chem Res* **2011,** *44* (10), 979-89; (b) Serda, R. E.; Godin, B.; Blanco, E.; Chiappini, C.; Ferrari, M., Multi-stage delivery nano-particle systems for therapeutic applications. *Biochim Biophys Acta* **2011,** *1810* (3), 317-29.

59. Decuzzi, P.; Godin, B.; Tanaka, T.; Lee, S. Y.; Chiappini, C.; Liu, X.; Ferrari, M., Size and shape effects in the biodistribution of intravascularly injected particles. *J Control Release* **2010,** *141* (3), 320-7.

60. Chiappini, C.; Tasciotti, E.; Fakhoury, J. R.; Fine, D.; Pullan, L.; Wang, Y. C.; Fu, L.; Liu, X.; Ferrari, M., Tailored porous silicon microparticles: fabrication and properties. *Chemphyschem* **2010,** *11* (5), 1029-35.

61. Ciro Chiappini; Ennio Tasciotti; Rita E. Serda; Lou Brousseau; Xuewu Liu; Ferrari, M., Mesoporous silicon particles as intravascular drug delivery vectors: fabrication, in-vitro, and in-vivo assessments. *physica status solidi* **2011,** *8* (6), 1826–1832.

62. Kolonin, M.; Pasqualini, R.; Arap, W., Molecular addresses in blood vessels as targets for therapy. *Curr Opin Chem Biol* **2001,** *5* (3), 308-13.

63. Serda, R. E.; Gu, J.; Bhavane, R. C.; Liu, X.; Chiappini, C.; Decuzzi, P.; Ferrari, M., The association of silicon microparticles with endothelial cells in drug delivery to the vasculature. *Biomaterials* **2009,** *30* (13), 2440-8.

64. Ferrati, S.; Mack, A.; Chiappini, C.; Liu, X.; Bean, A. J.; Ferrari, M.; Serda, R. E., Intracellular trafficking of silicon particles and logic-embedded vectors. *Nanoscale* **2010,** *2* (8), 1512-20.

65. Domhan, S.; Ma, L.; Tai, A.; Anaya, Z.; Beheshti, A.; Zeier, M.; Hlatky, L.; Abdollahi, A., Intercellular communication by exchange of cytoplasmic material via tunneling nano-tube like structures in primary human renal epithelial cells. *PLoS One* **2011,** *6* (6), e21283.

66. Gurke, S.; Barroso, J. F.; Gerdes, H. H., The art of cellular communication: tunneling nanotubes bridge the divide. *Histochem Cell Biol* **2008,** *129* (5), 539-50.

67. Mi, L.; Xiong, R.; Zhang, Y.; Li, Z.; Yang, W.; Chen, J.; Wang, P., Microscopic Observation of the Intercellular Transport of CdTe Quantum Do. *Journal of Biomaterials and Nanobiotechnology* **2011,** *2*, 173-180.

68. Serda, R. E.; Mack, A.; Pulikkathara, M.; Zaske, A. M.; Chiappini, C.; Fakhoury, J. R.; Webb, D.; Godin, B.; Conyers, J. L.; Liu, X. W.; Bankson, J. A.; Ferrari, M., Cellular association and assembly of a multistage delivery system. *Small* **2010,** *6* (12), 1329-40.

69. Tanaka, T.; Godin, B.; Bhavane, R.; Nieves-Alicea, R.; Gu, J.; Liu, X.; Chiappini, C.; Fakhoury, J. R.; Amra, S.; Ewing, A.; Li, Q.; Fidler, I. J.; Ferrari, M., In vivo evaluation of safety of nanoporous silicon carriers following single and multiple dose intravenous administrations in mice. *Int J Pharm* **2010,** *402* (1-2), 190-7.

70. (a) Swanson, J. A.; Yirinec, B. D.; Silverstein, S. C., Phorbol esters and horseradish peroxidase stimulate pinocytosis and redirect the flow of pinocytosed fluid in macrophages. *J Cell Biol* **1985,** *100* (3), 851-9; (b) Buckmaster, M. J.; Lo Braico, D., Jr.; Ferris, A. L.; Storrie, B., Retention of pinocytized solute by CHO cell lysosomes correlates with molecular weight. *Cell Biol Int Rep* **1987,** *11* (7), 501-7.

71. Vogel, S. M.; Minshall, R. D.; Pilipovic, M.; Tiruppathi, C.; Malik, A. B., Albumin uptake and transcytosis in endothelial cells in vivo induced by albumin-binding protein. *Am J Physiol Lung Cell Mol Physiol* **2001,** *281* (6), L1512-22.

72. Matsushita, K.; Yamakuchi, M.; Morrell, C. N.; Ozaki, M.; O'Rourke, B.; Irani, K.; Lowenstein, C. J., Vascular endothelial growth factor regulation of Weibel-Palade-body exocytosis. *Blood* **2005,** *105* (1), 207-14.

73. (a) Valentijn, K. M.; Sadler, J. E.; Valentijn, J. A.; Voorberg, J.; Eikenboom, J., Functional architecture of Weibel-Palade bodies. *Blood* **2011,** *117* (19), 5033-43; (b) Valentijn, K. M.; van Driel, L. F.; Mourik, M. J.; Hendriks, G. J.; Arends, T. J.; Koster, A. J.; Valentijn, J. A., Multigranular exocytosis of Weibel-Palade bodies in vascular endothelial cells. *Blood* **2010,** *116* (10), 1807-16.

74. Martina, M. S.; Fortin, J. P.; Menager, C.; Clement, O.; Barratt, G.; Grabielle-Madelmont, C.; Gazeau, F.; Cabuil, V.; Lesieur, S., Generation of superparamagnetic liposomes revealed as highly efficient MRI contrast agents for in vivo imaging. *J Am Chem Soc* **2005,** *127* (30), 10676-85.

75. Jain, R. K.; Stylianopoulos, T., Delivering nanomedicine to solid tumors. *Nat Rev Clin Oncol* **2010,** *7* (11), 653-64.

6 Vita

Silvia Ferrati was born in Florence, Italy on June 22, 1981, the Daughter of Rossella Gori and Maurizio Ferrati.

After completing her work at A. Gramsci High School, Florence, Italy in 2000, she entered University of Florence in Florence, Italy. She received the degree of Master of Science with a major in physical-chemistry from the University of Florence in May, 2006.

She then entered University of Venice (CIVEN program) in Venice, Italy, from which she received her degree of Master of Science with a major in nanotechnology in December 2007, after the completion of her internship in the Department of Biomedical Engineering of The University of Texas Health Science Center at Houston.

In January 2008, she entered The University of Texas Health Science Center at Houston Graduate School of Biomedical Sciences as a graduate student.

Permanent address:

2120 El Paseo, Apt. #2804

Houston, Texas 77054

USA